

# Structure and Kinematics of the central BLR in AGN

Wolfram Kollatschny, Göttingen

Divcibare, 2011

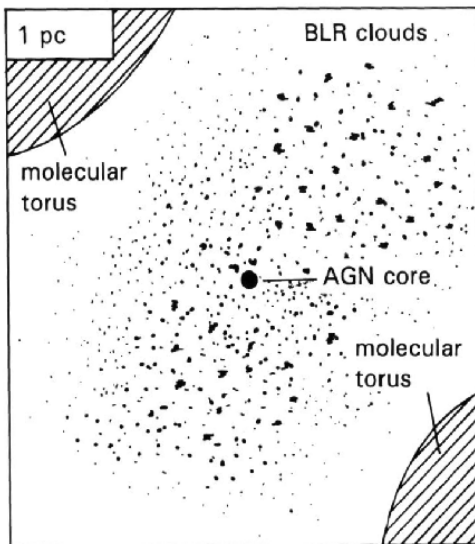


University Observatory

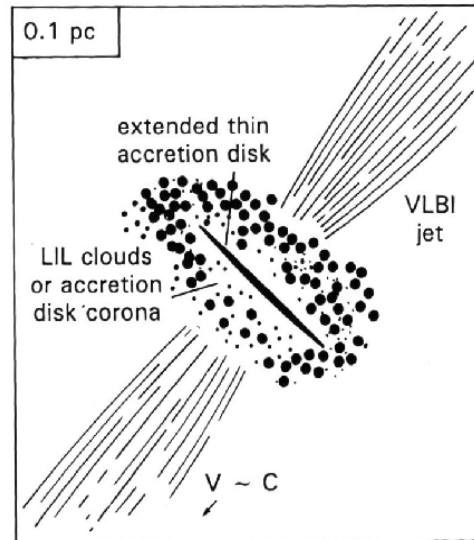


Institute for Astrophysics

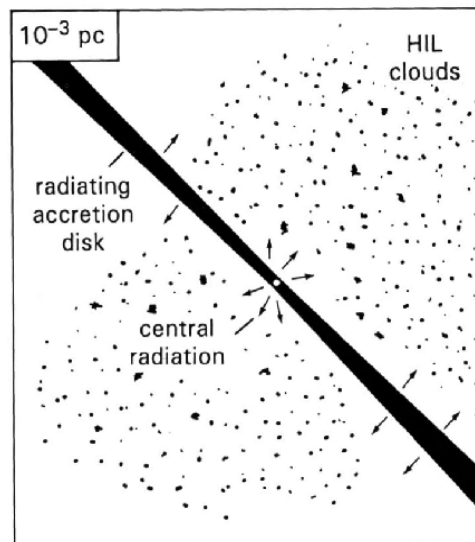
# Broad Line Region Size?



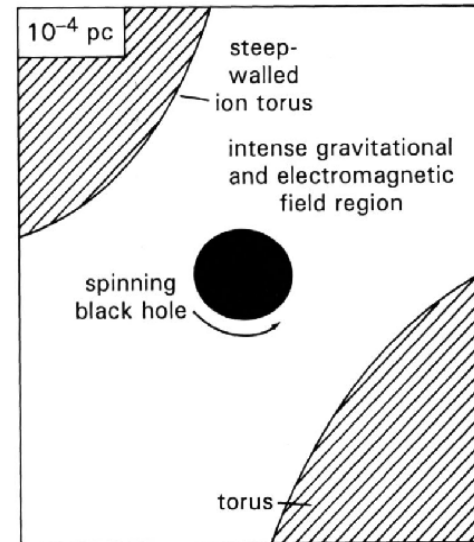
The outer extent of the broad-line region and the deep-walled molecular torus which can provide an effective shield of the central AGN, depending on the relative orientation of the observer.



Inside the molecular torus — the VLBI jet becomes self-absorbed closer in, and the low ionization lines of the BLR, which might be the corona of the accretion disk.



The accretion disk which radiates strongly at UV and optical wavelengths. The high ionization clouds of the BLR are excited by the central continuum radiation field.



The black hole. The Schwarzschild radius for a  $10^8 M_{\odot}$  black hole is 2 AU ( $10^{-5}$  pc). The spin will introduce twisted magnetic field lines and particle acceleration.

radius:

-  $10^{-4} \dots 10^{-1}$  pc

- 1 .... 100 light days

at a dist. of 50 Mpc (Virgo):  
spatial resolution

$4 \times 10^{-5} \dots 4 \times 10^{-3}$  ''  
(0.04 ... 4. mas)

unresolved

R. Blandford

# Broad Line Region Structure?

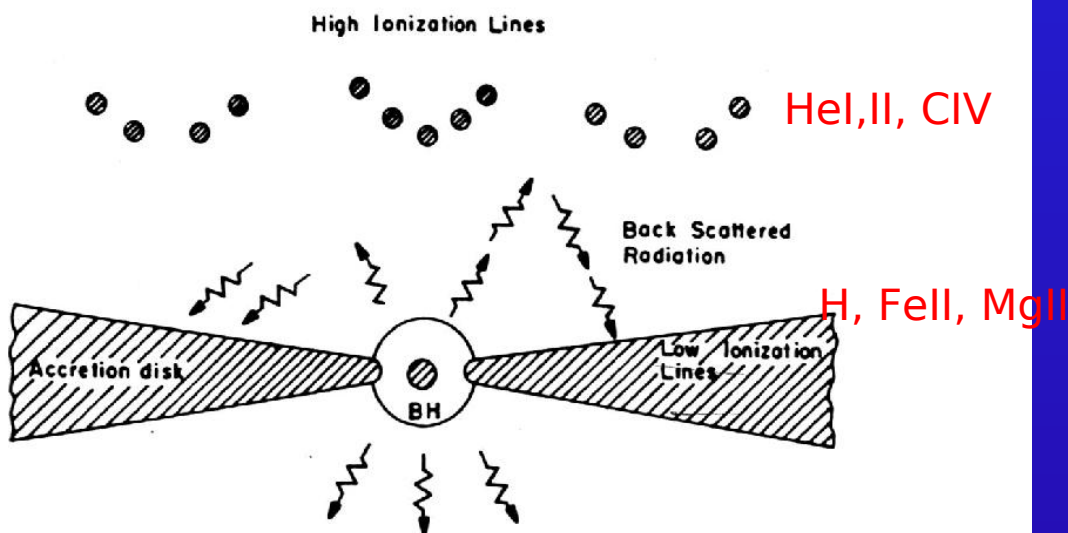
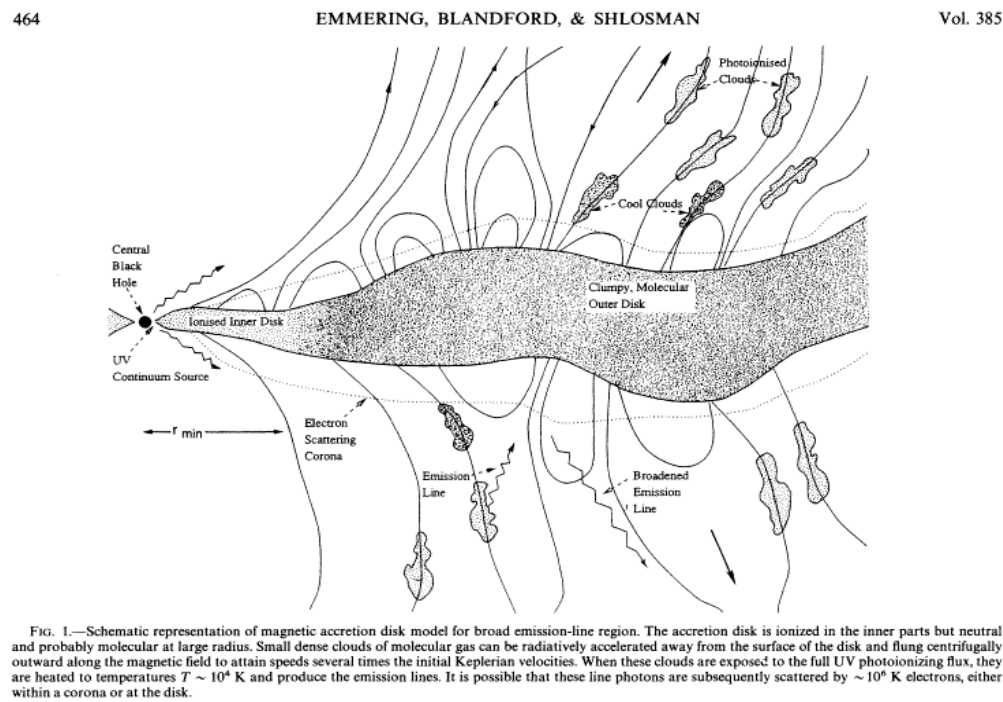


**Fig. 13.** A schematic two-component model for the BLR. The high ionization lines are emitted in a spherical system of clouds, and are excited by the direct ultraviolet radiation of the central source. The low ionization lines come mainly from the outer regions of the central disk, where most of the line excitation is due to back-scattered, hard ionizing photons. (After Collin-Souffrin, Perry and Dyson(1987), Collin-Souffrin (1987) and Dumont and Collin-Souffrin (1990))

Two component BLR?

Collin-Souffrin et al., 1990



Radiatively accelerated clouds in hydromagnetic wind?

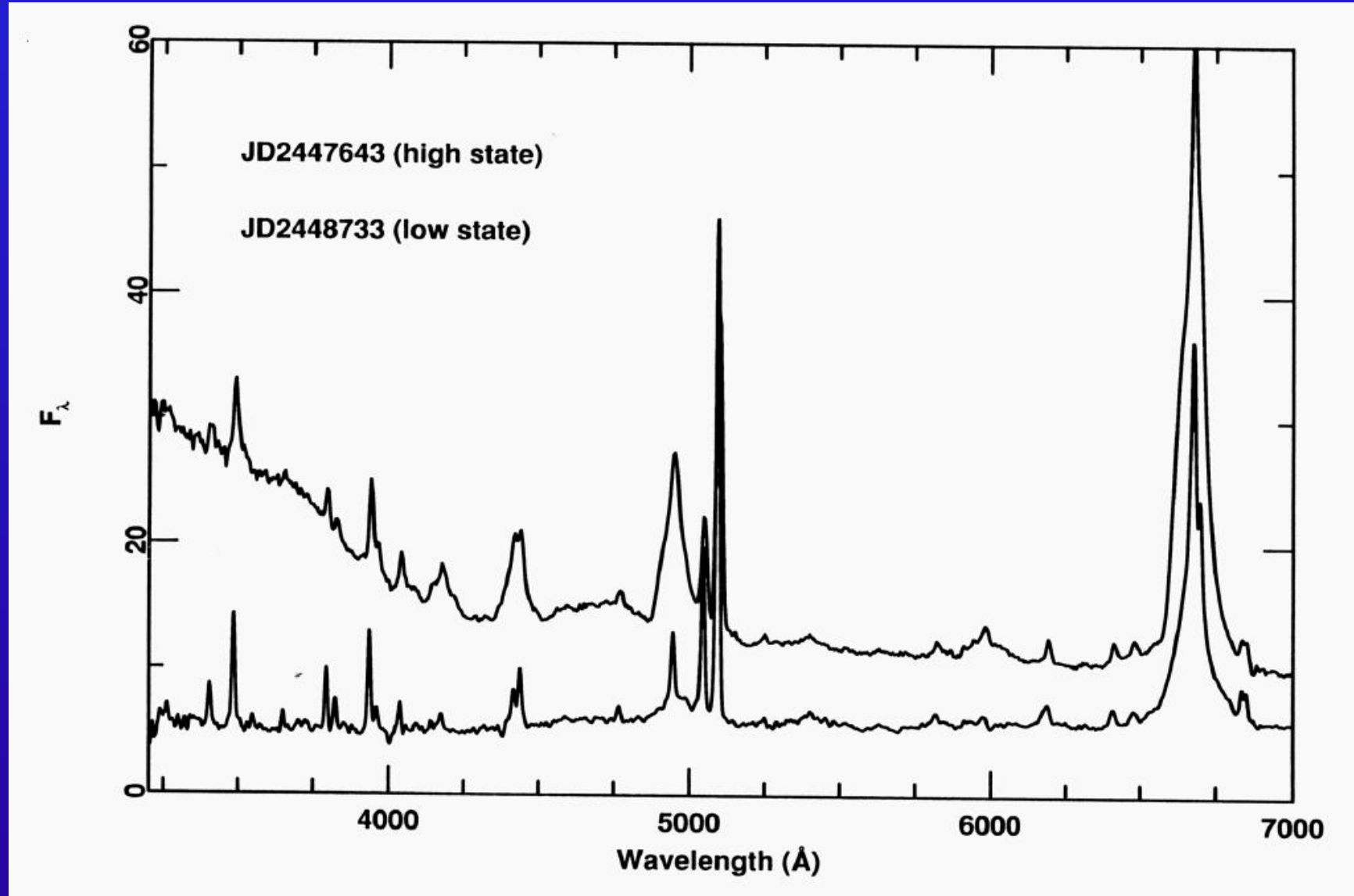
Emmering, Blandford, Shlosman, 1992

# Study of Variability:

- Extension, Structure*
- Geometry*
- and Kinematics* of the central  
Broad Line Region in AGN
  
- *Black Hole Mass*

in NGC5548, Mrk110

# High and low state spectra of NGC5548

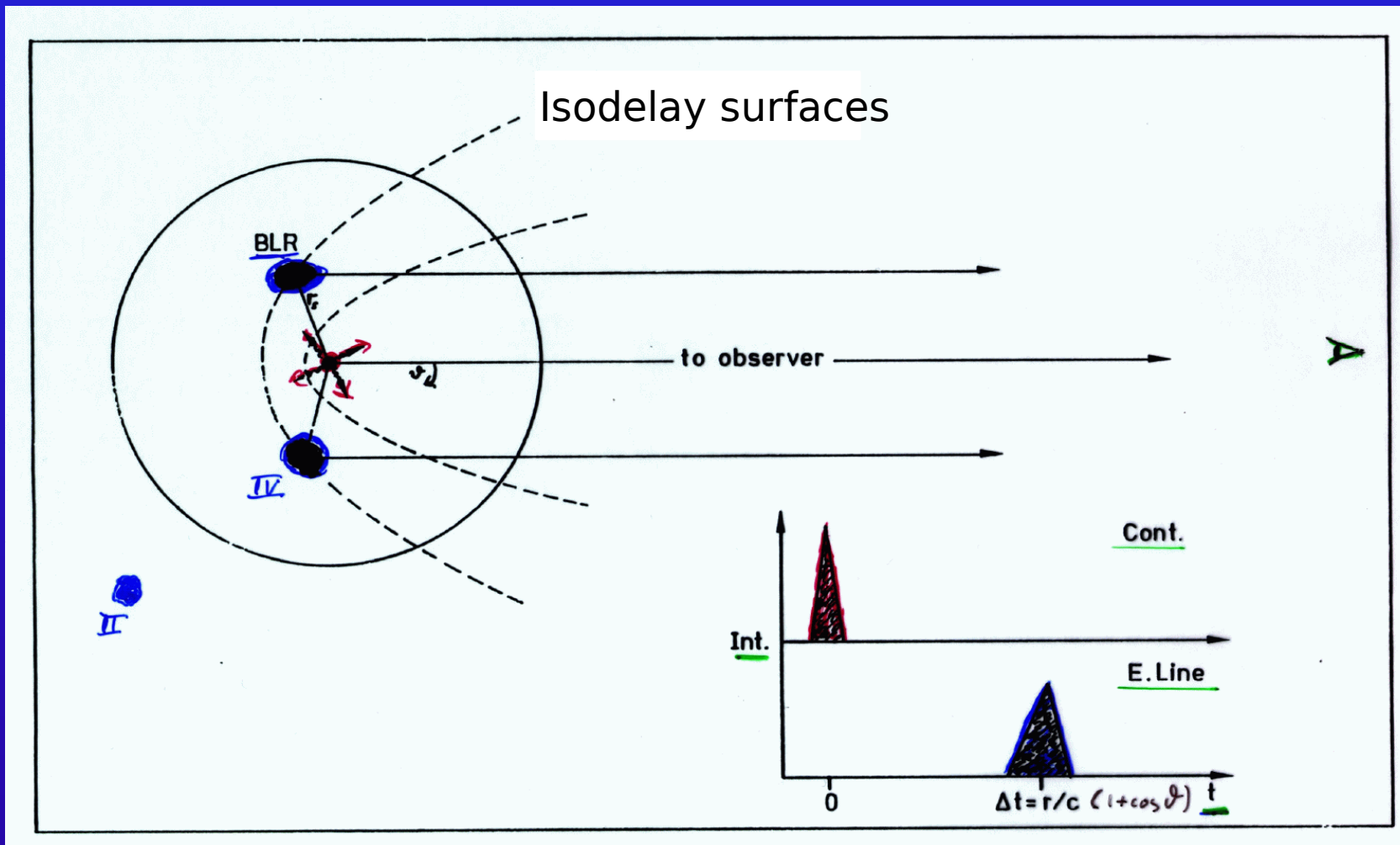


1989

1993

# BLR: Idealized Model

*Response of BLR clouds on continuum flashes*



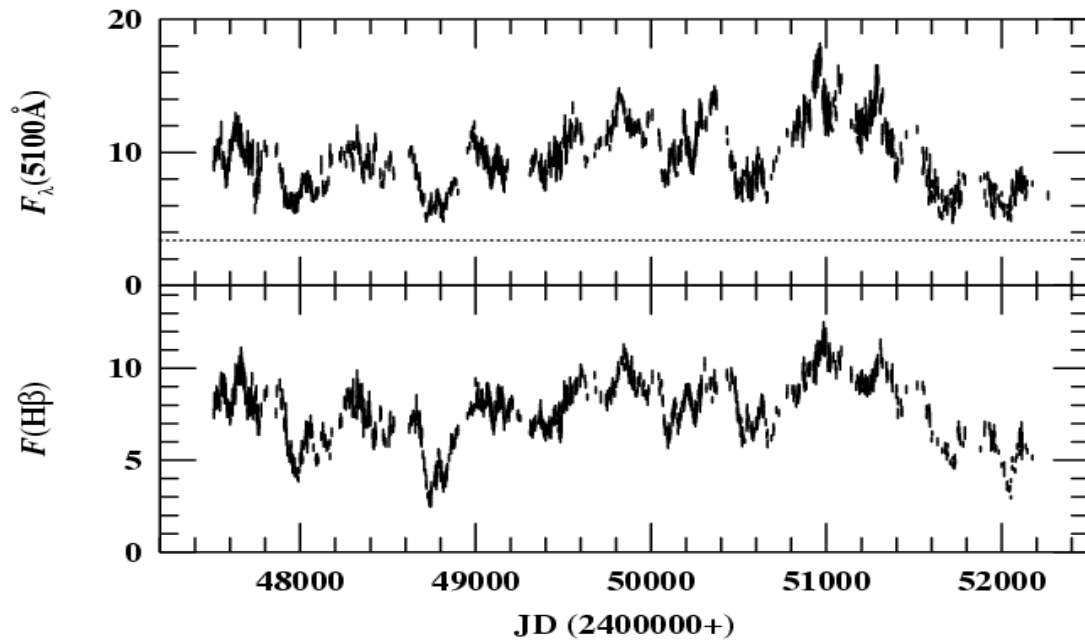
BLR stratification

Delay by light travel time effects

# BLR: Continuum & integ. $H\beta$ line variability

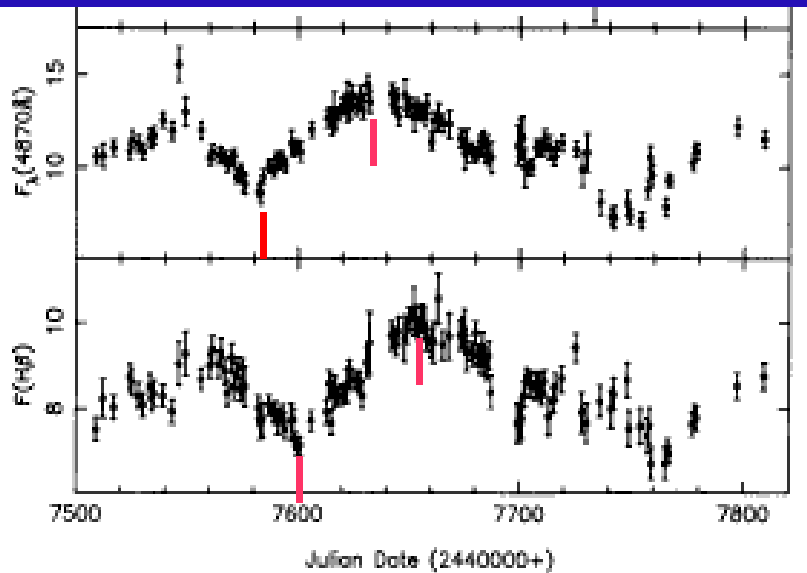
1989 - 2001

NGC 5548



B. Peterson et al., 2002

$H\beta$  delay  $\sim 20$  light days



1989

# BLR size and stratification in NGC5548

peak to peak  
var. ampl.

lightcurves (1989)

ACF, CCF

opt. Cont.

0.56

H $\beta$

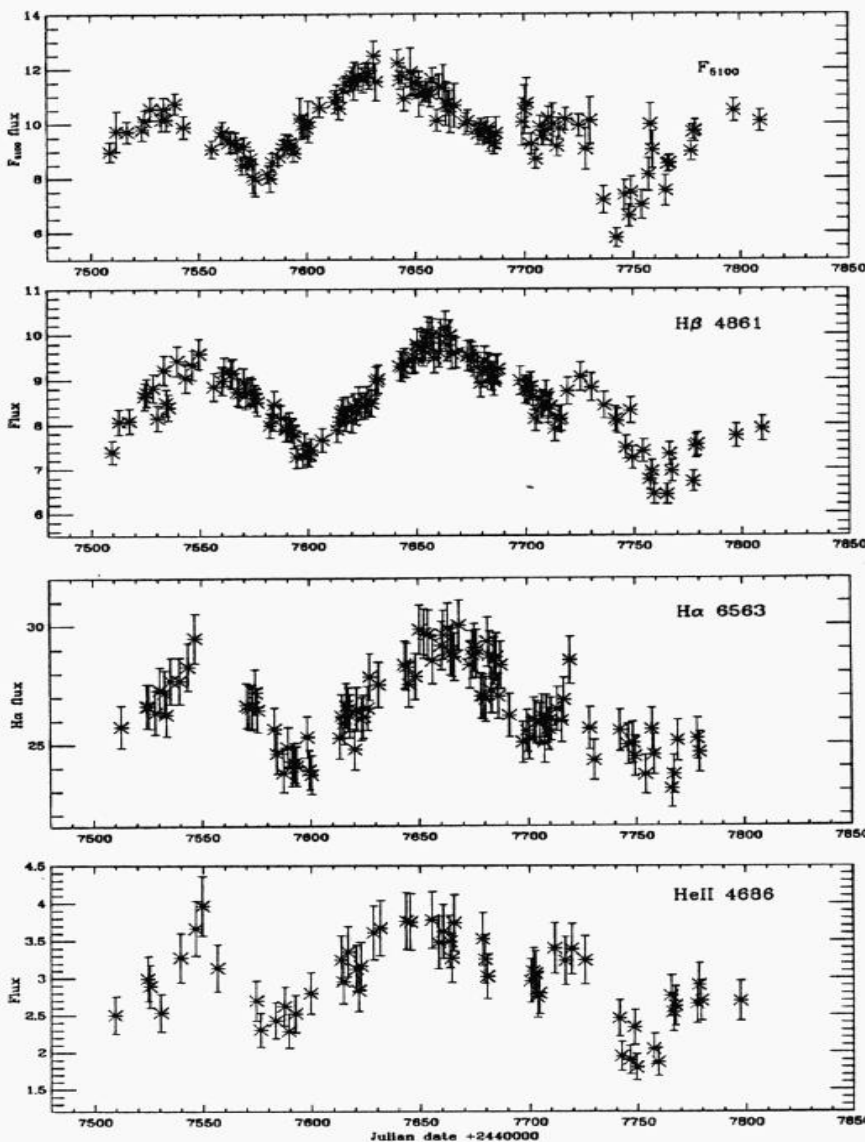
0.29

H $\alpha$

(0.17)

Hell

0.61



delay

H $\beta$

19.

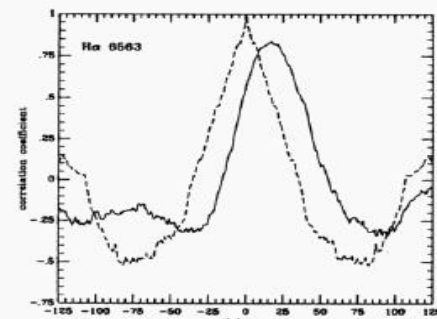
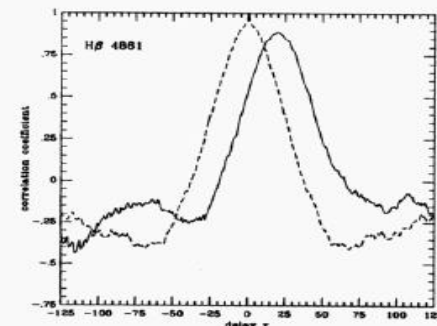
H $\alpha$

(18.)

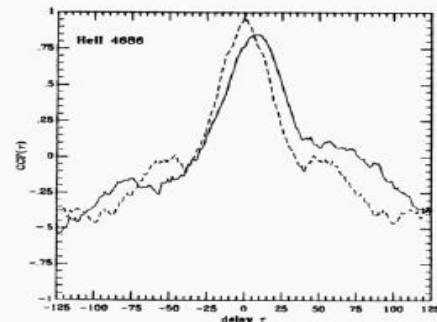
Hell

7.

Correlation coeff.



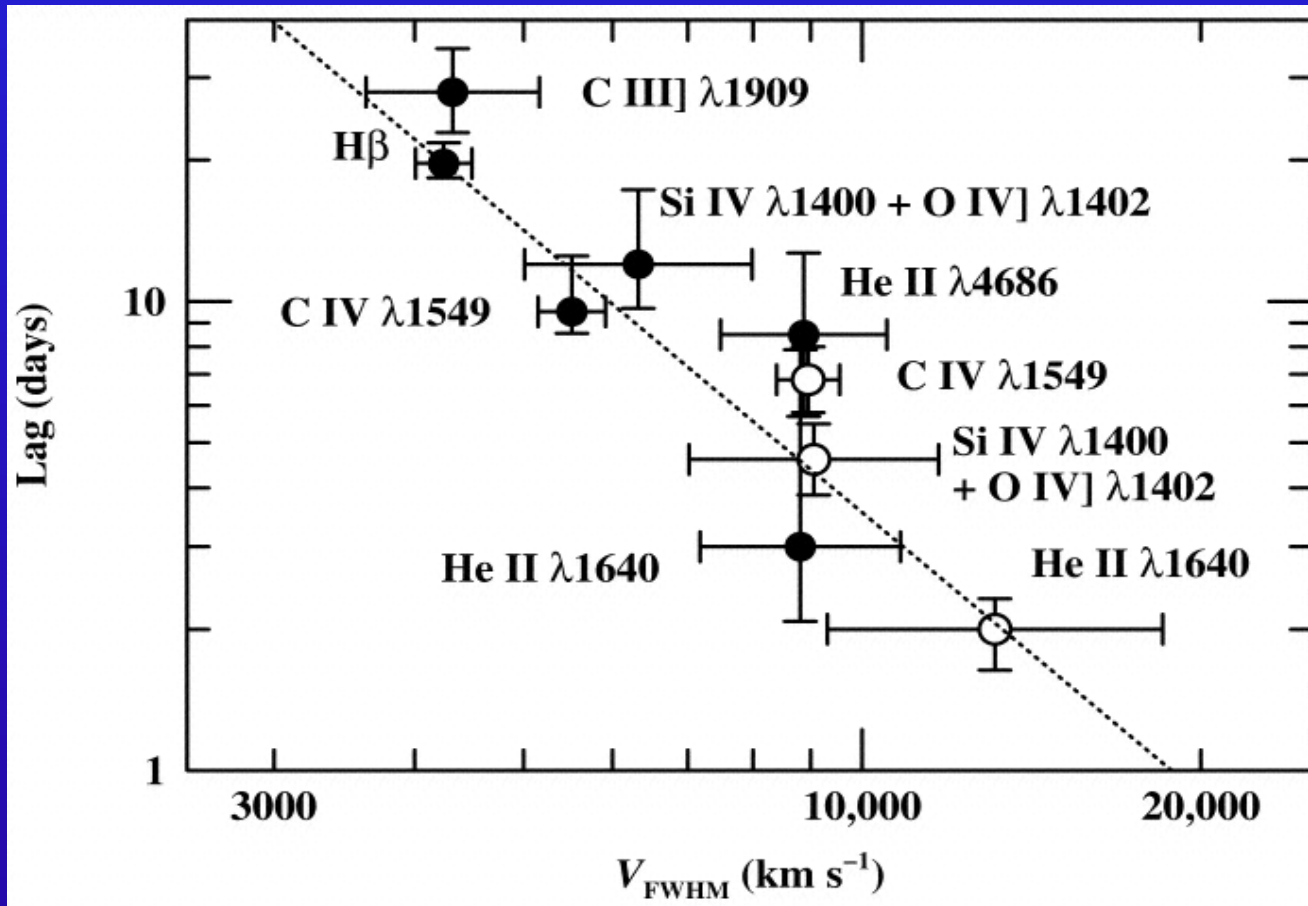
Delay  $\tau$  [days]





# BLR size and stratification in NGC5548

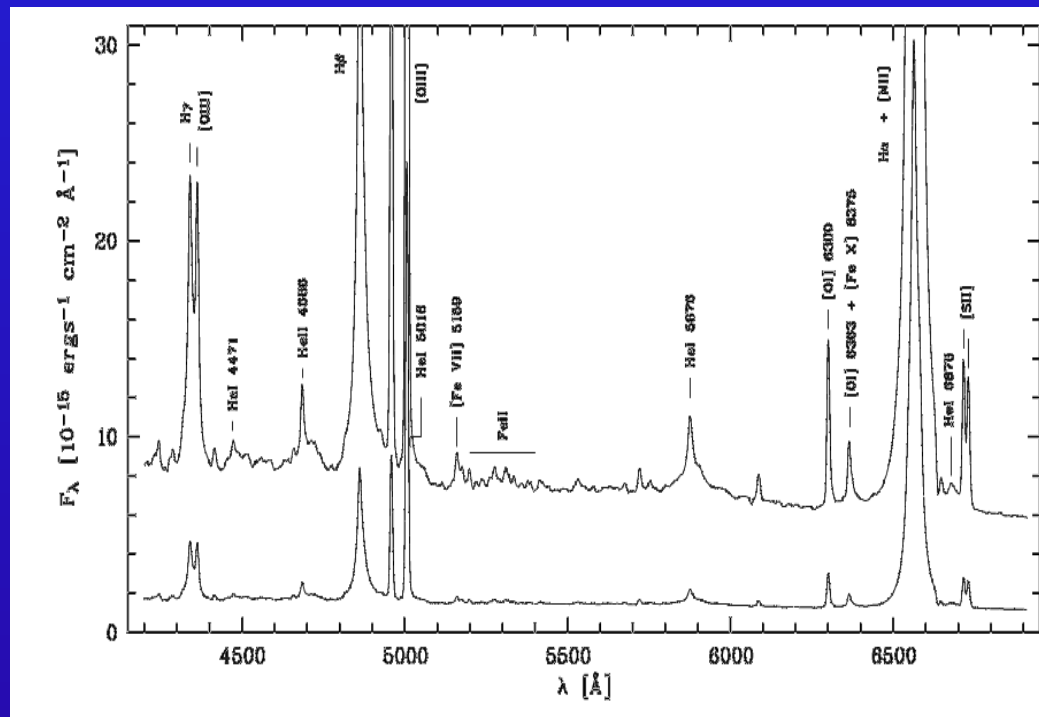
higher ionized lines: - broader line widths  
- faster response



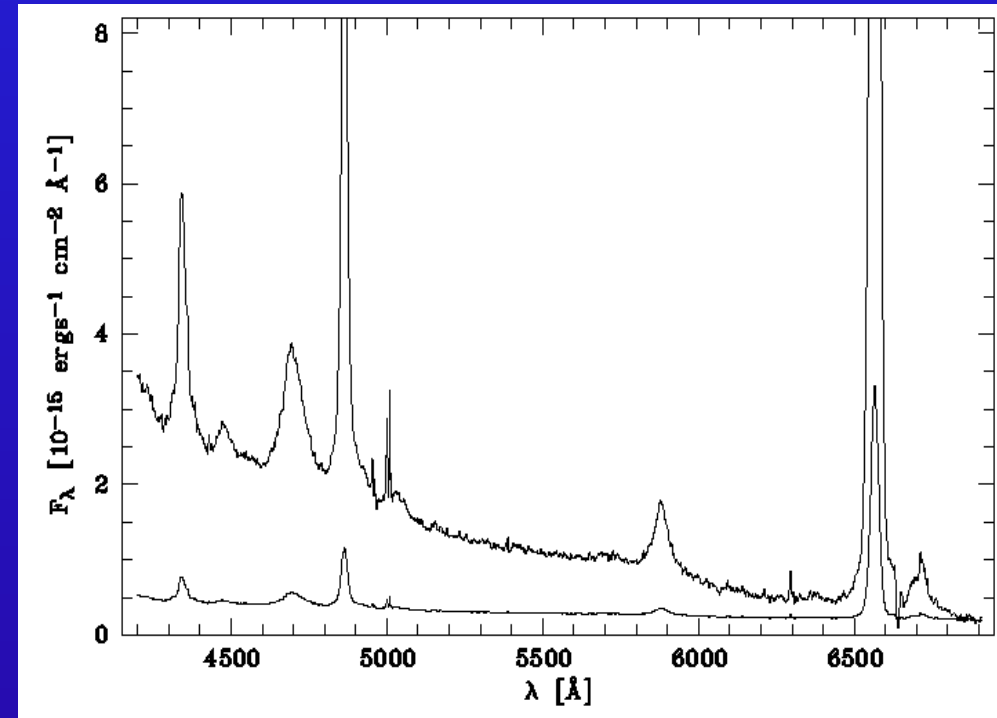
Time lag (CCFs centroids) for various emission lines

# HET variability campaign of Mrk110

9.2m Hobby-Eberly Telescope at McDonald Observatory  
S/N >100



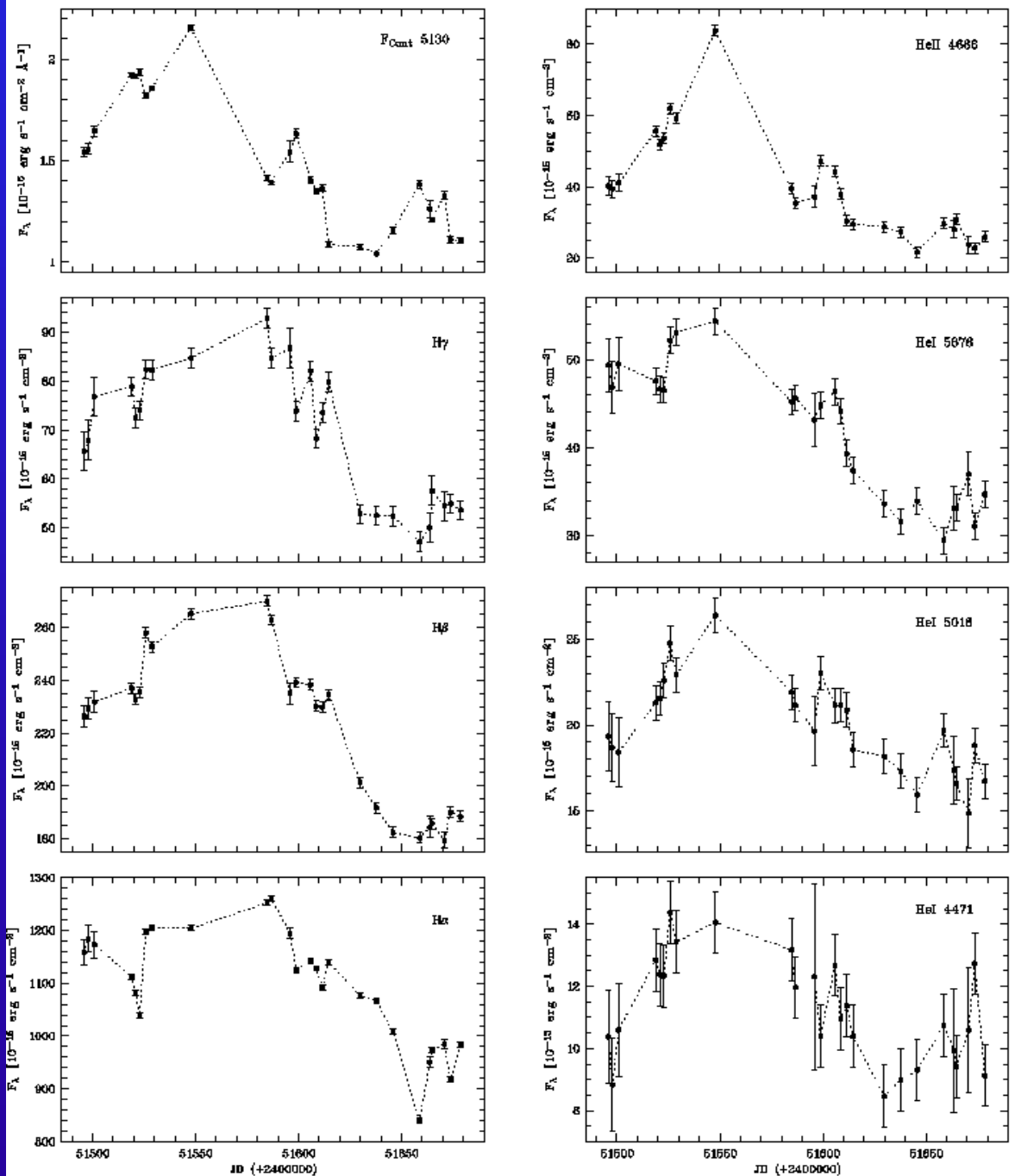
Mean spectrum of Mrk110  
for 24 epochs from Nov. 1999 through  
May 2000



Rms spectrum

- the rms spectrum shows the  
variable part of the spectrum

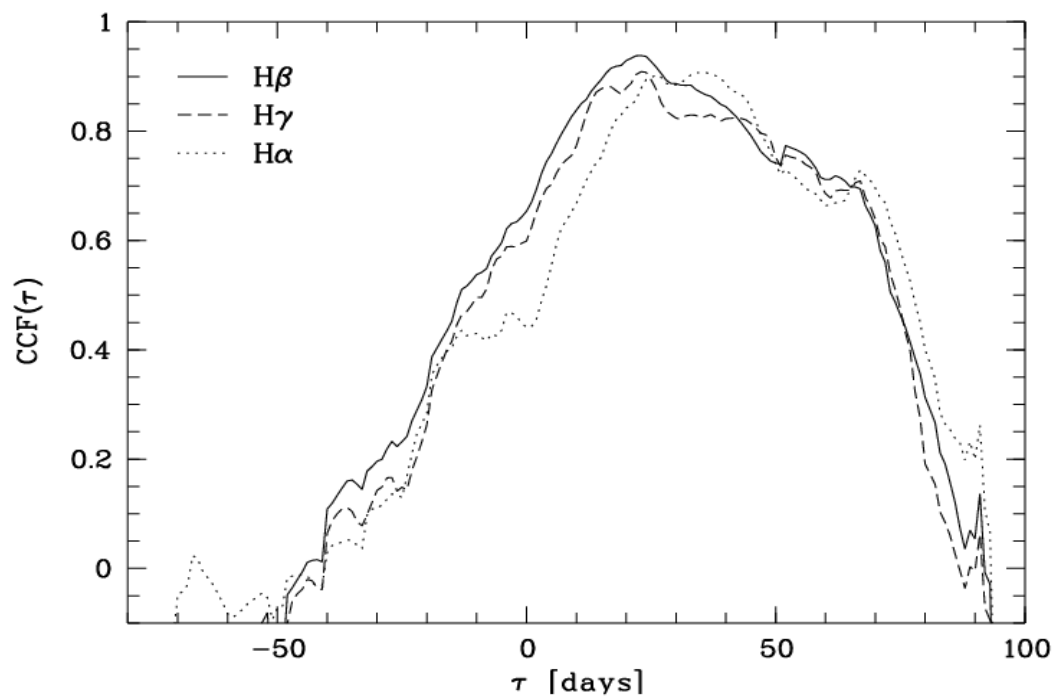
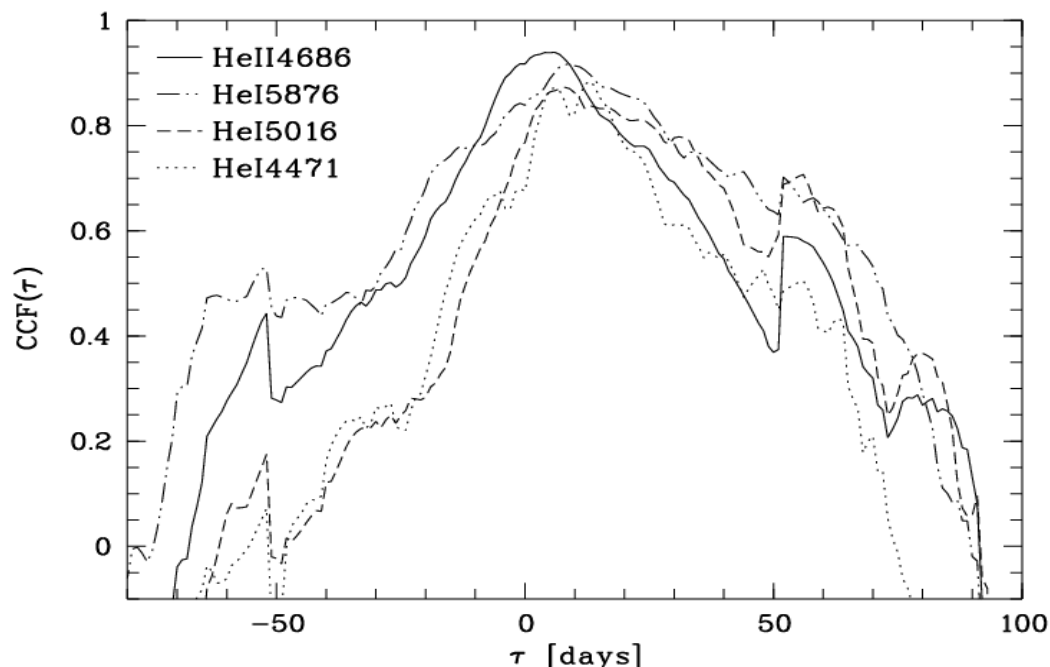
# HET variability campaign of Mrk110



Continuum and integrated emission line (Balmer, HeII and HeI) light curves

1999 Nov. - 2000 May

# BLR size and structure - HET variab. campaign



Mkn110

CCF functions of HeII, HeI and Balmer line light curves with continuum light curve.

Line	$\tau_{cent}$ [days]
(1)	(2)
HeII $\lambda$ 4686	$3.9^{+2.8}_{-0.7}$
HeI $\lambda$ 4471	$11.1^{+6.0}_{-6.0}$
HeI $\lambda$ 5016	$14.3^{+7.0}_{-7.0}$
HeI $\lambda$ 5876	$10.7^{+8.0}_{-6.0}$
H $\gamma$	$26.5^{+4.6}_{-4.7}$
H $\beta$	$24.2^{+3.7}_{-3.3}$
H $\alpha$	$32.3^{+4.3}_{-4.9}$

stratification

# Central Black Hole Mass in Mrk110

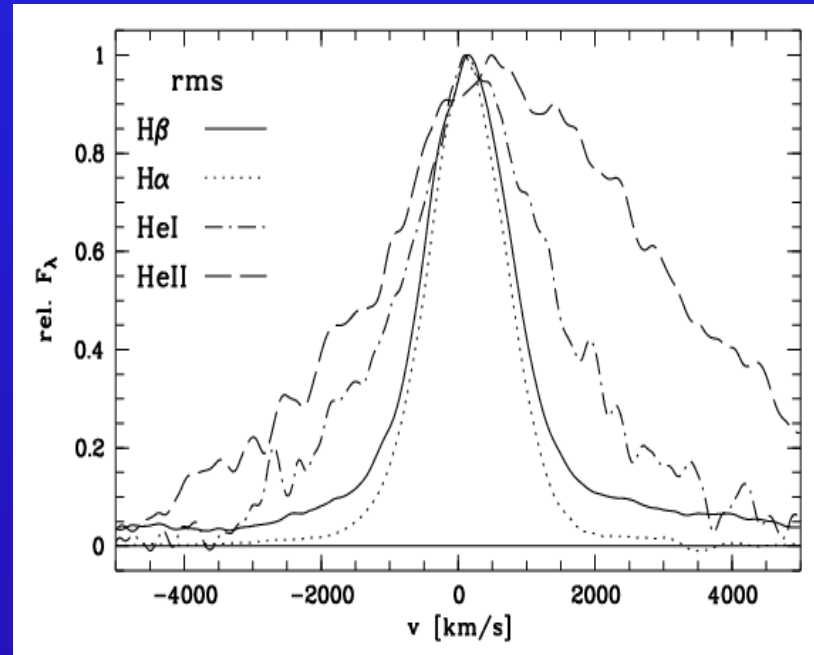
Assumption:  
emission line clouds  
are gravitationally bound by  
central object

$$M = \frac{fV_{\text{FWHM}}^2 c\tau}{G}$$

$c\tau$  = mean dist. of  
line em. clouds

$V$  = vel. disp. of clouds  
(from rms line width)

$f$  = factor ( $\frac{1}{2}$  - 5.5)  
(unknown geometry)

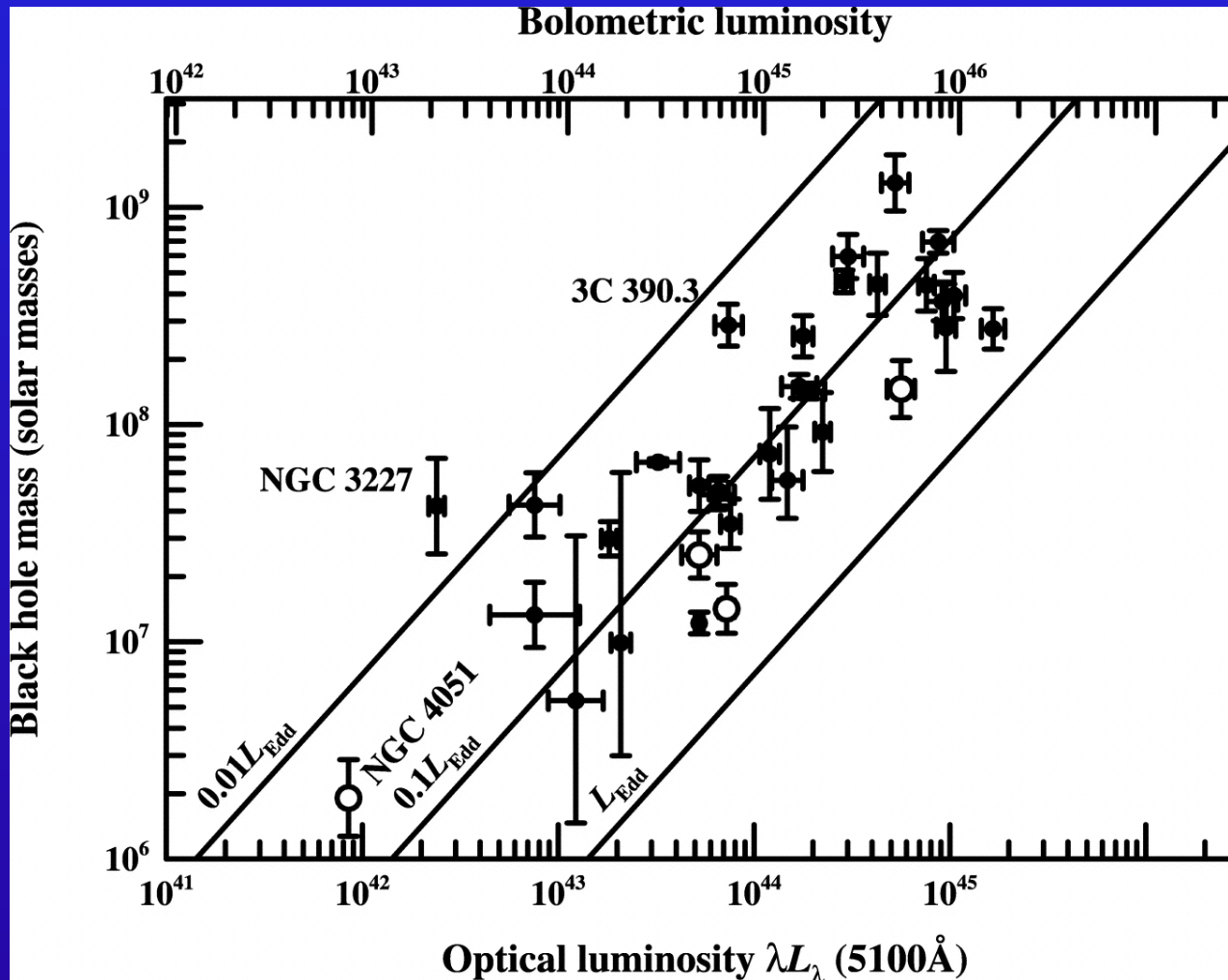


Normalized rms line profiles in velocity space

Line	FWHM(rms) [km s <sup>-1</sup> ]	$\tau_{\text{cent}}$ [days]	$M$ [10 <sup>7</sup> M <sub>⊙</sub> ]
(1)	(2)	(3)	(4)
HeIIλ4686	4444. ± 200	3.5 <sup>+2.</sup> <sub>-2.</sub>	2.25 <sup>+1.63</sup> <sub>-0.45</sub>
HeIλ5876	2404. ± 100	10.8 <sup>+4.</sup> <sub>-4.</sub>	1.81 <sup>+1.36</sup> <sub>-0.33</sub>
Hβ	1515. ± 100	23.5 <sup>+4.</sup> <sub>-4.</sub>	1.63 <sup>+0.33</sup> <sub>-0.31</sub>
Hα	1315. ± 100	32.5 <sup>+4.</sup> <sub>-4.</sub>	1.64 <sup>+0.33</sup> <sub>-0.35</sub>

# Central Black Hole Masses in AGN

## Black hole mass vs. luminosity for AGN

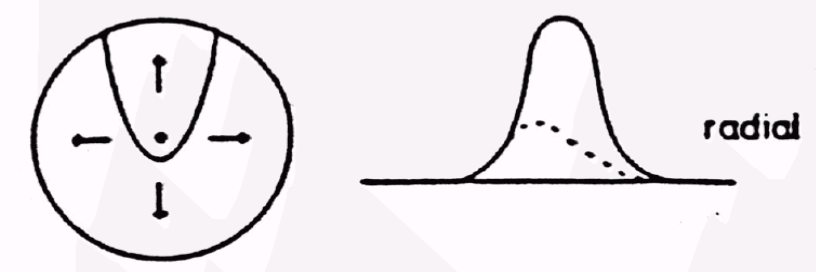
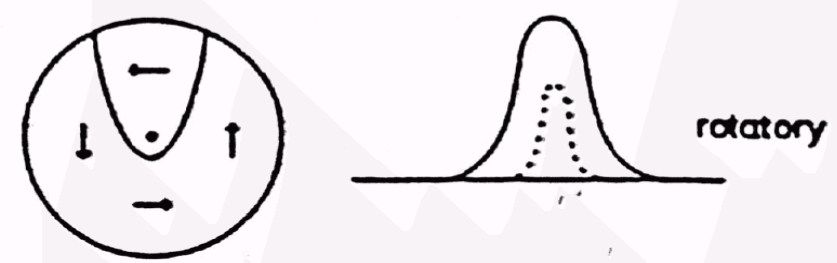
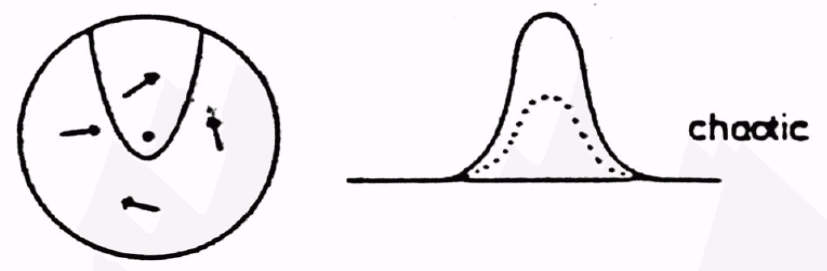


BH mass for 35 reverberation mapped AGN.

--- : lines of constant mass to luminosity ratio  
open circles: NLSy1

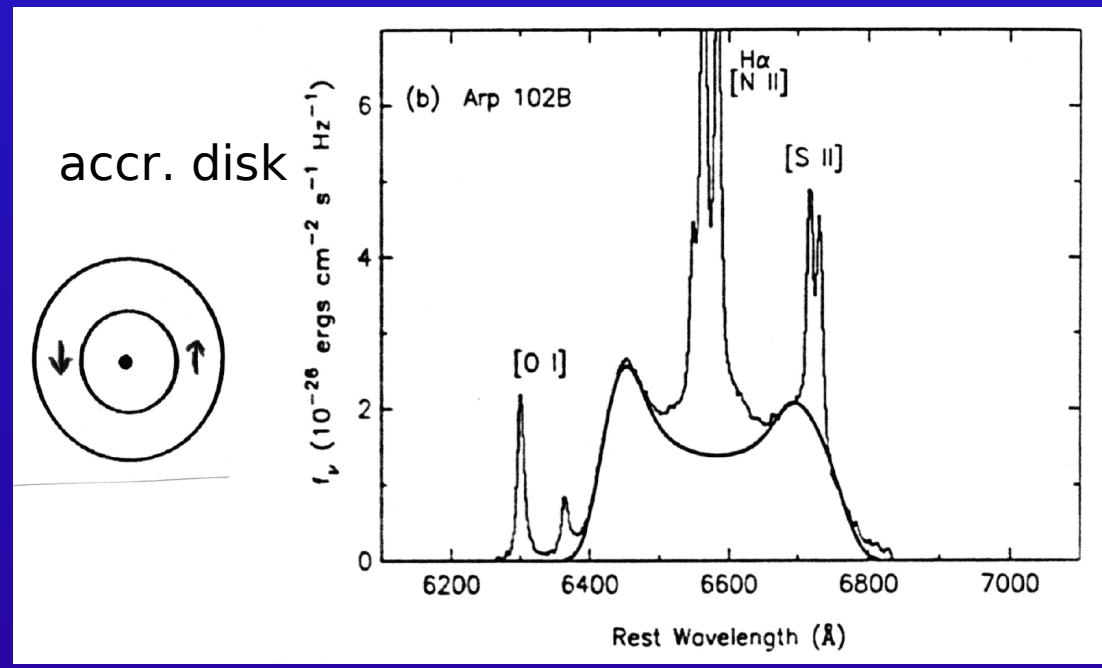
Peterson et al., 2004

# BLR kinematics - line profile variations



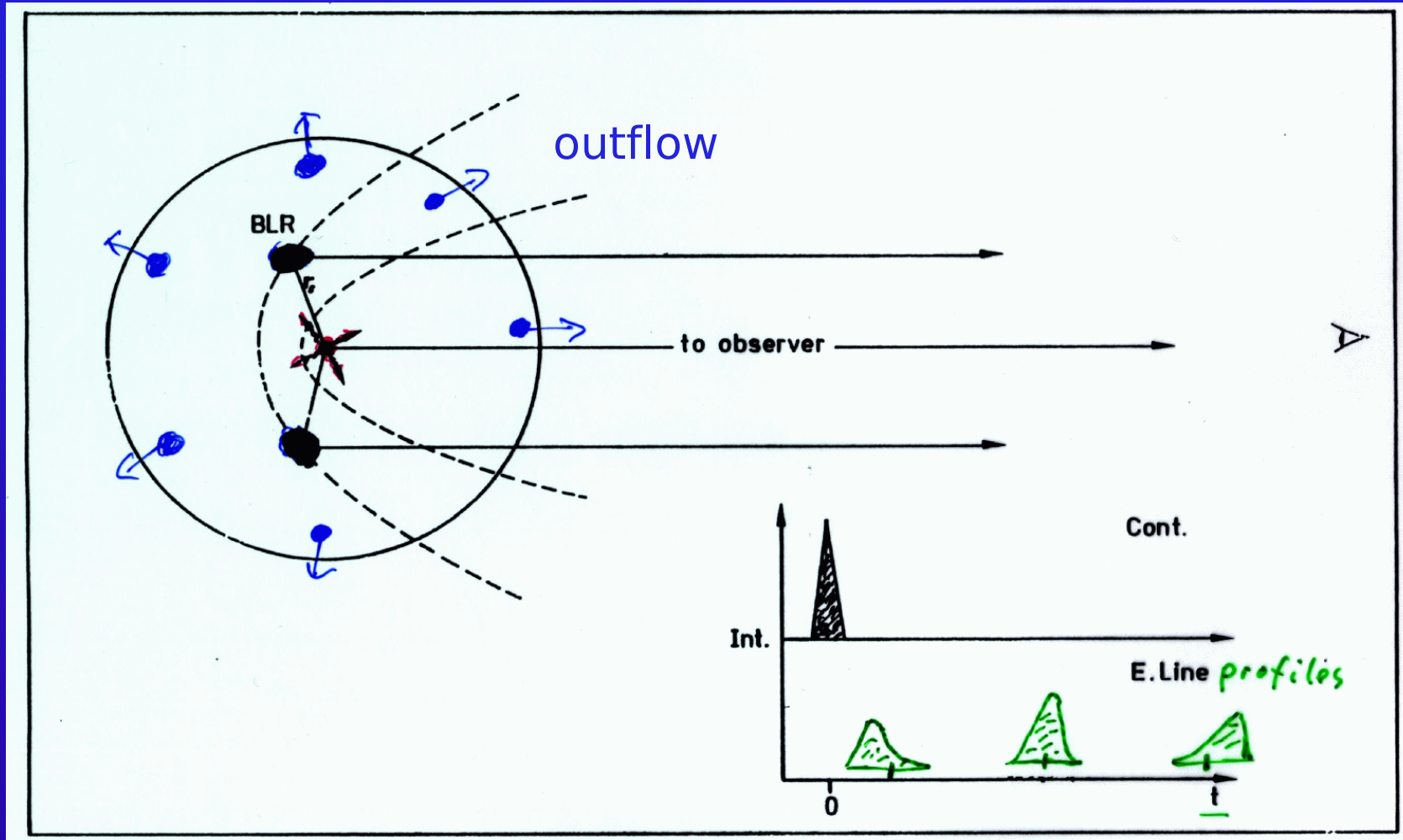
— profile at maximum  
 ..... profile early in outburst

Information about kinematics:  
 - from emission line profile variations  
 - from line profiles



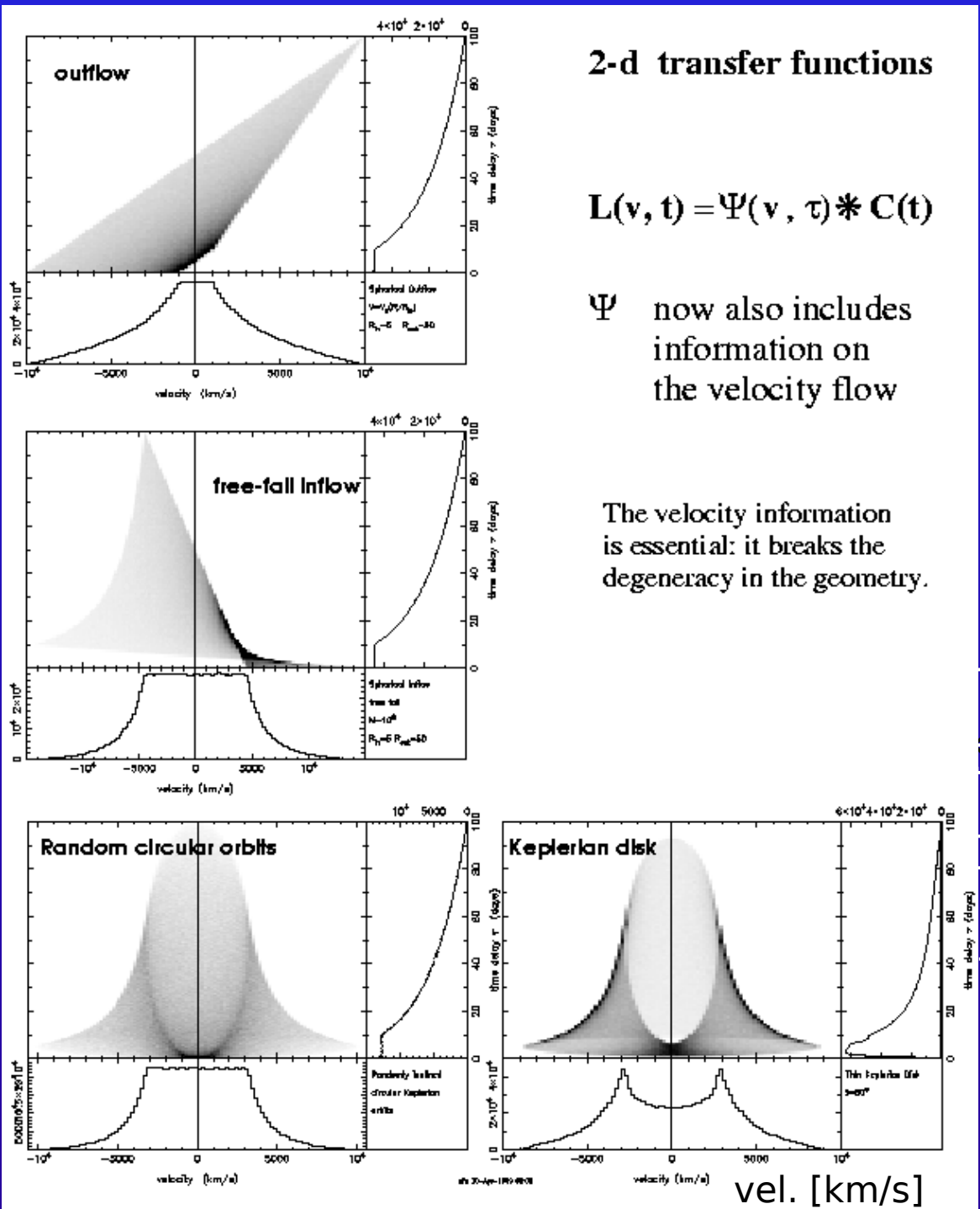
# BLR Kinematics: Idealized Model

Influence of BLR motions on line profile variations





# Theory : BLR kinematics - line profile variations



2-d transfer functions

$$L(v, t) = \Psi(v, \tau) * C(t)$$

$\Psi$  now also includes information on the velocity flow

The velocity information is essential: it breaks the degeneracy in the geometry.

theoretical emission line profile variations to derive 2-dim. velocity-delay maps  $\Psi$

velocity-delay maps for different flows

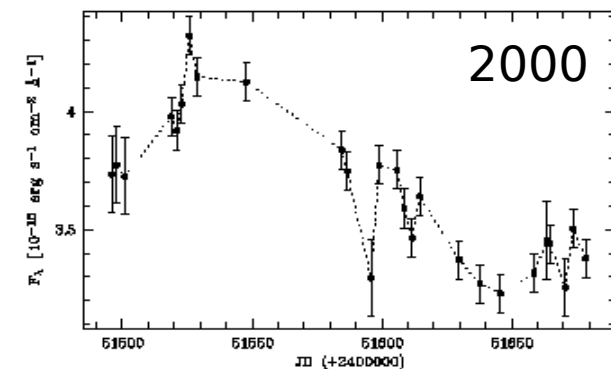
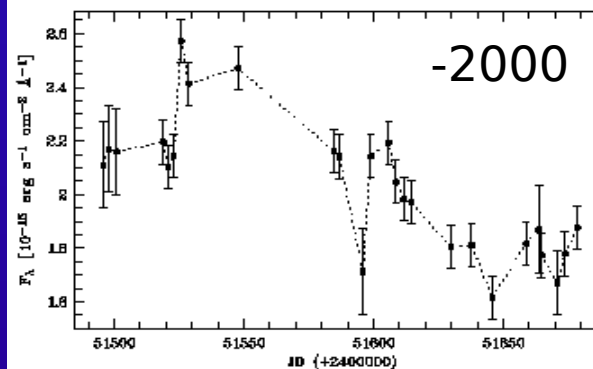
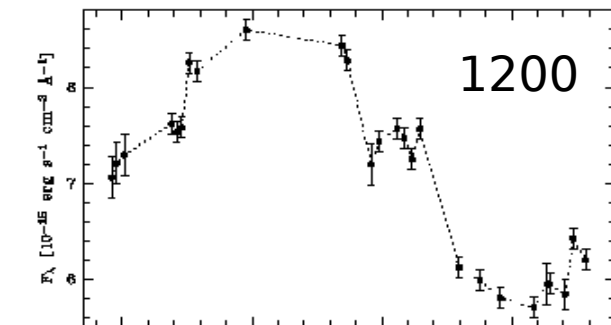
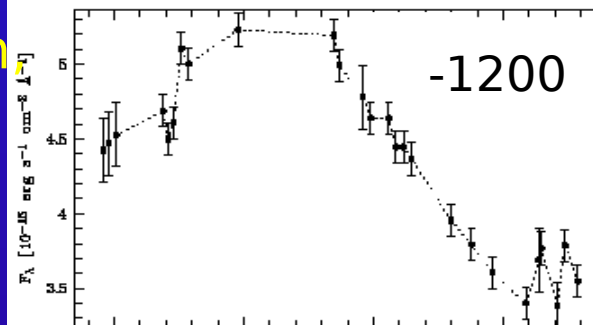
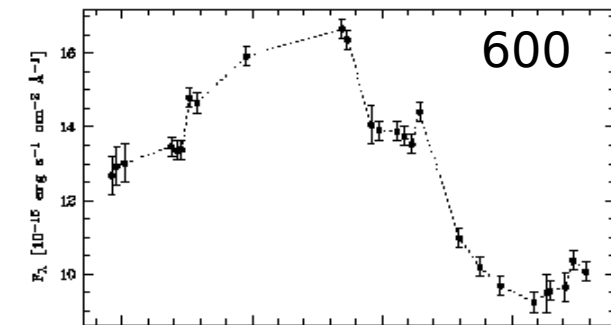
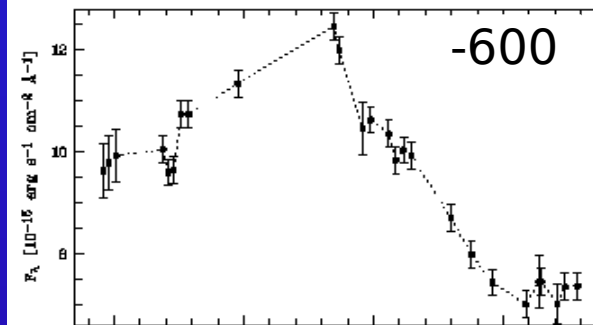
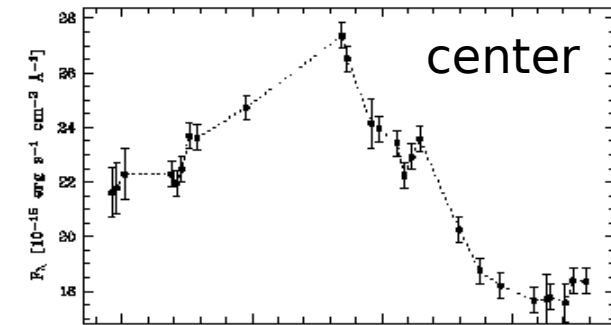
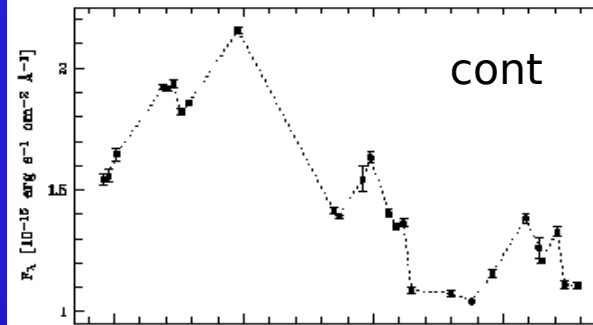
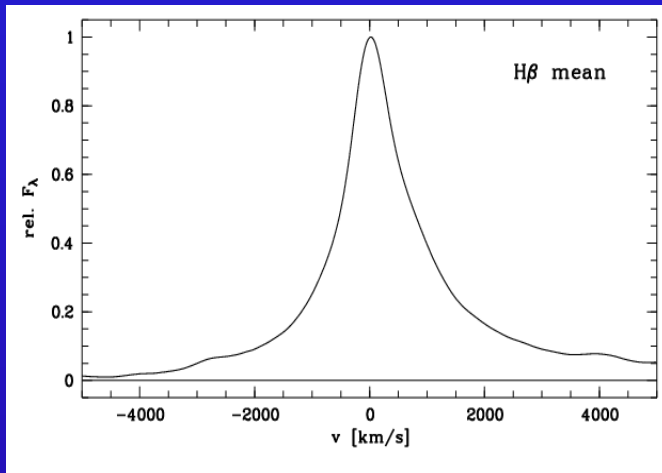
time delay [days]

Welsh & Horne, 1991  
Horne et al., 2004

vel. [km/s]

# BLR kinematics and accretion disk structure

Mean H $\beta$  line profile of Mrk110 in velocity space

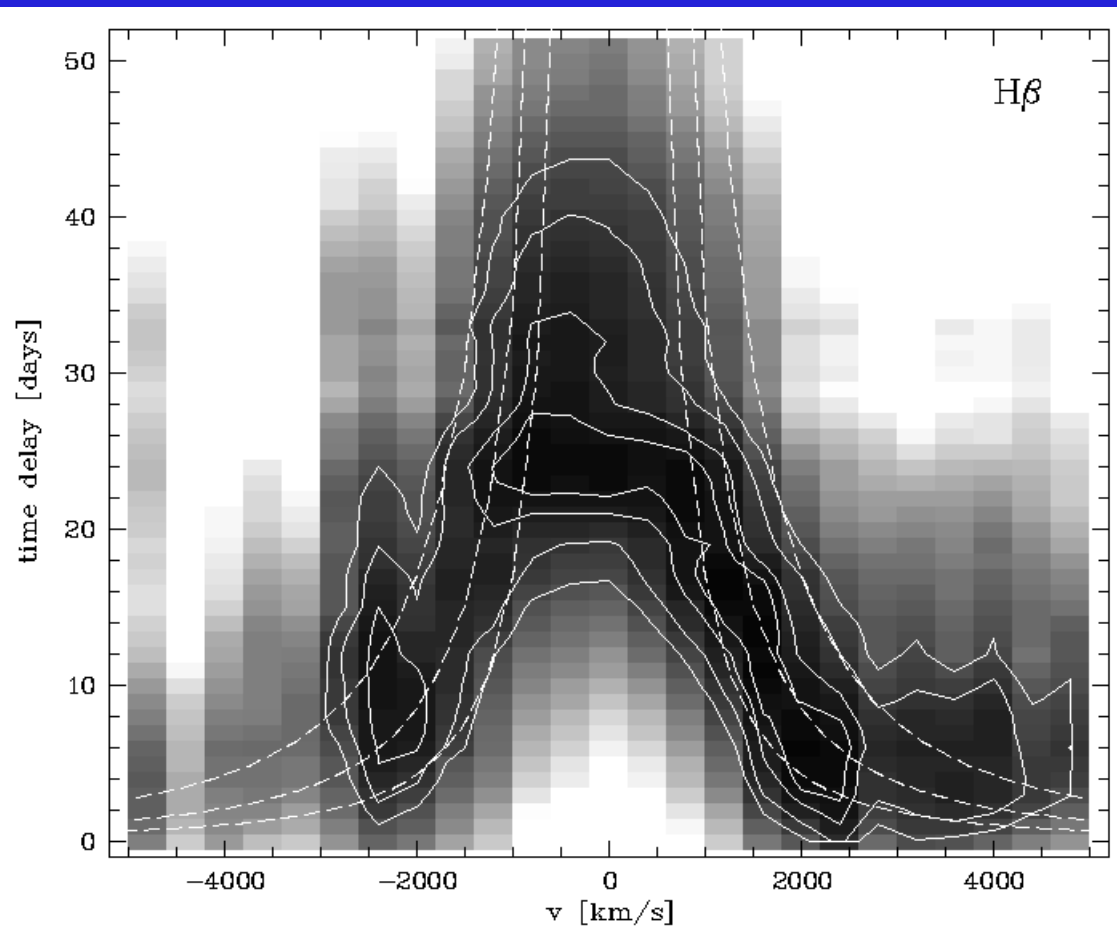


Light curves of the continuum of the H $\beta$  line center, and of different blue and red line wing segments

$$\Delta v = 400 \text{ km/s}$$

Kollatschny & Bischoff 2002

# BLR: Accretion disk structure in Mrk110



2-D CCF : correlation of H $\beta$  line profile segments with cont. variations (grey scale)

Contours of correlation coefficient at levels of .85 to .925 (solid lines).

Dashed curves: theoretical escape velocity envelopes for masses of 0.5, 1., 2.  $10^7 M_{\odot}$  (from bottom to top).

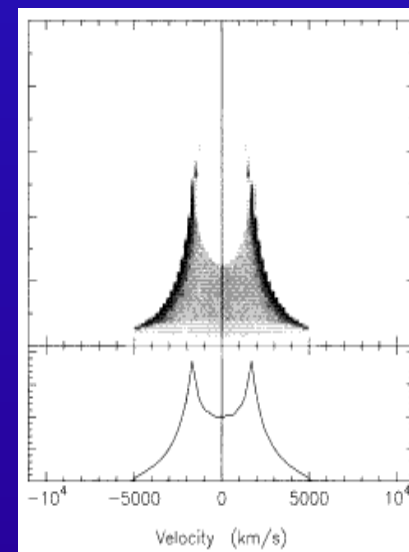
Velocity-delay map

Kollatschny 2003a

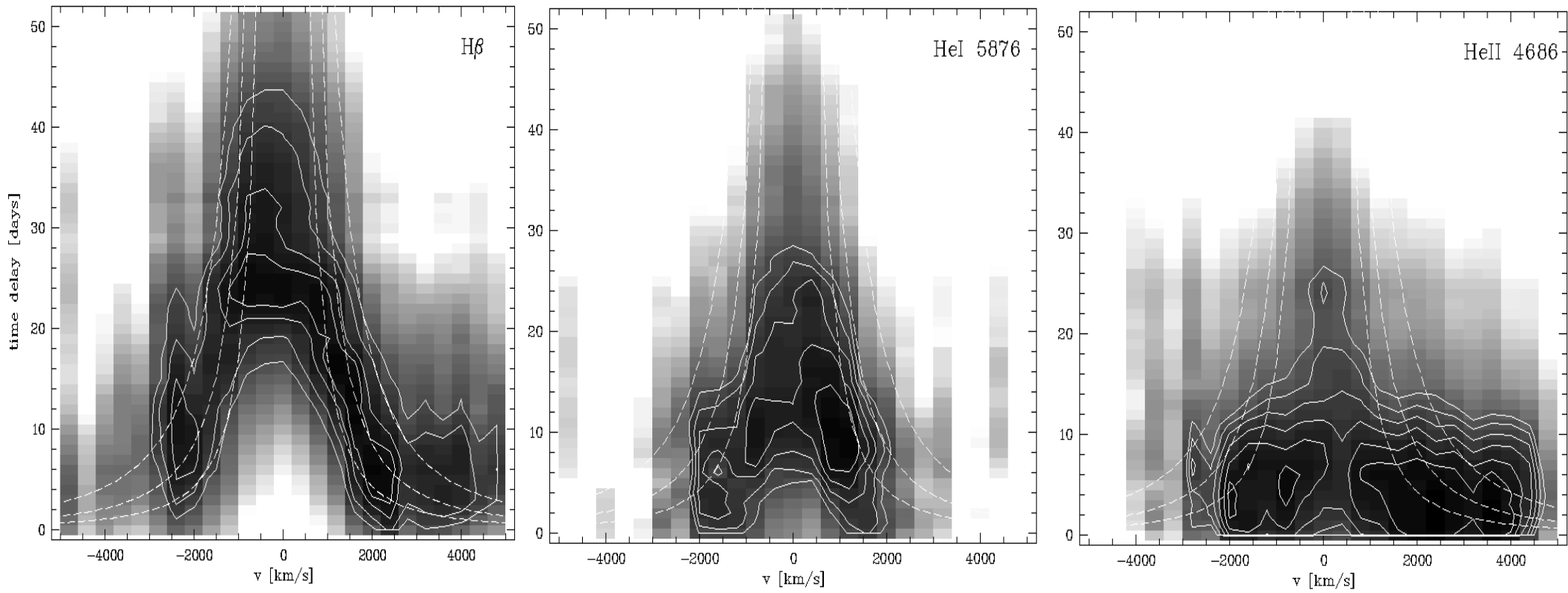
Theoretical velocity-delay maps for different flows:  
Keplerian disk BLR model: fast response of **both** outer line wings

Welsh & Horne 1991, Horne et al. 2004

Echo image



# Velocity-delay maps: accretion disk structure

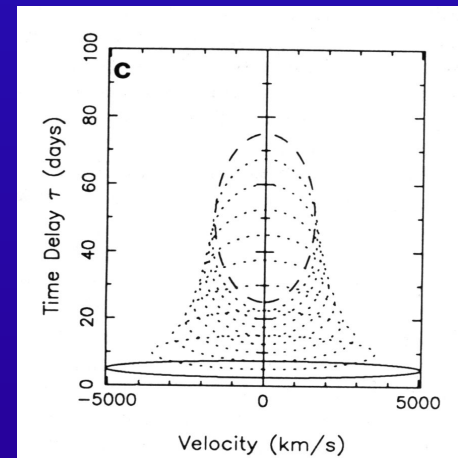
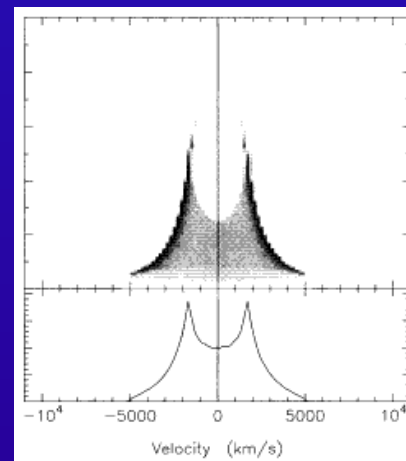


2-D CCF : correlation of H $\beta$ , HeI, HeII line profile segments with continuum variations (grey scale).

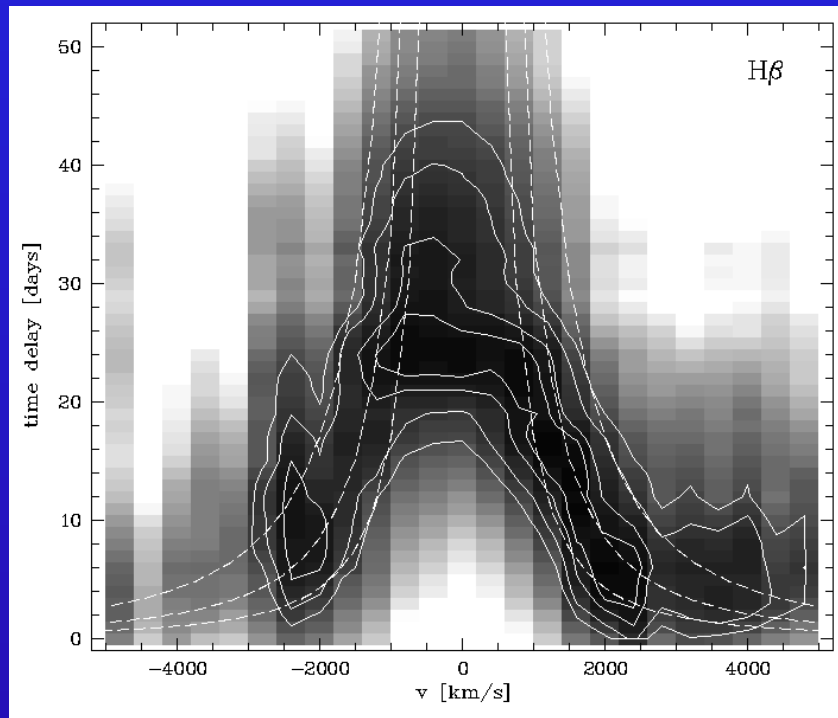
Kollatschny 2003

Keplerian disk BLR model: fast response of **both** outer line wings

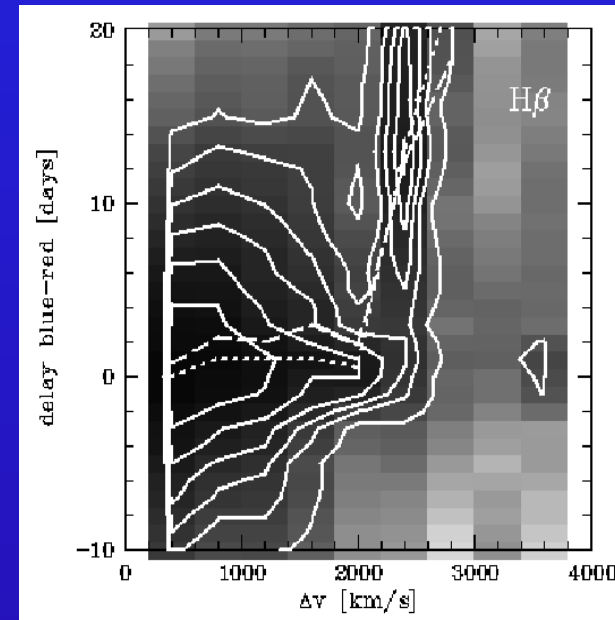
Solid line: innermost radius at  $5 l_d$



# BLR: Accretion disk wind in Mrk110



2-D CCF: velocity-delay map



Time delay of blue line wing to red line wing as function of dist. to line center

Outer line wings: inner BLR

Disk wind model of BLR: Slightly faster and stronger resonance of red wing  
Chiang & Murray, 1996

Disk driven outflow models compared to spherical wind models:  
velocity decreases with radius (rather than the other way around)

Koenigl & Kartje, 1994

# BLR Structure and Kinematics in Mrk110

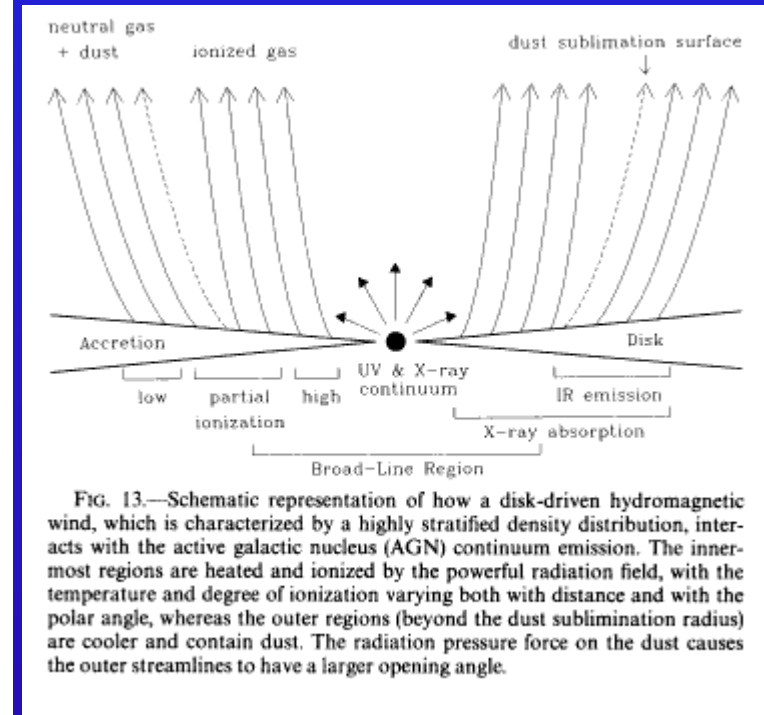
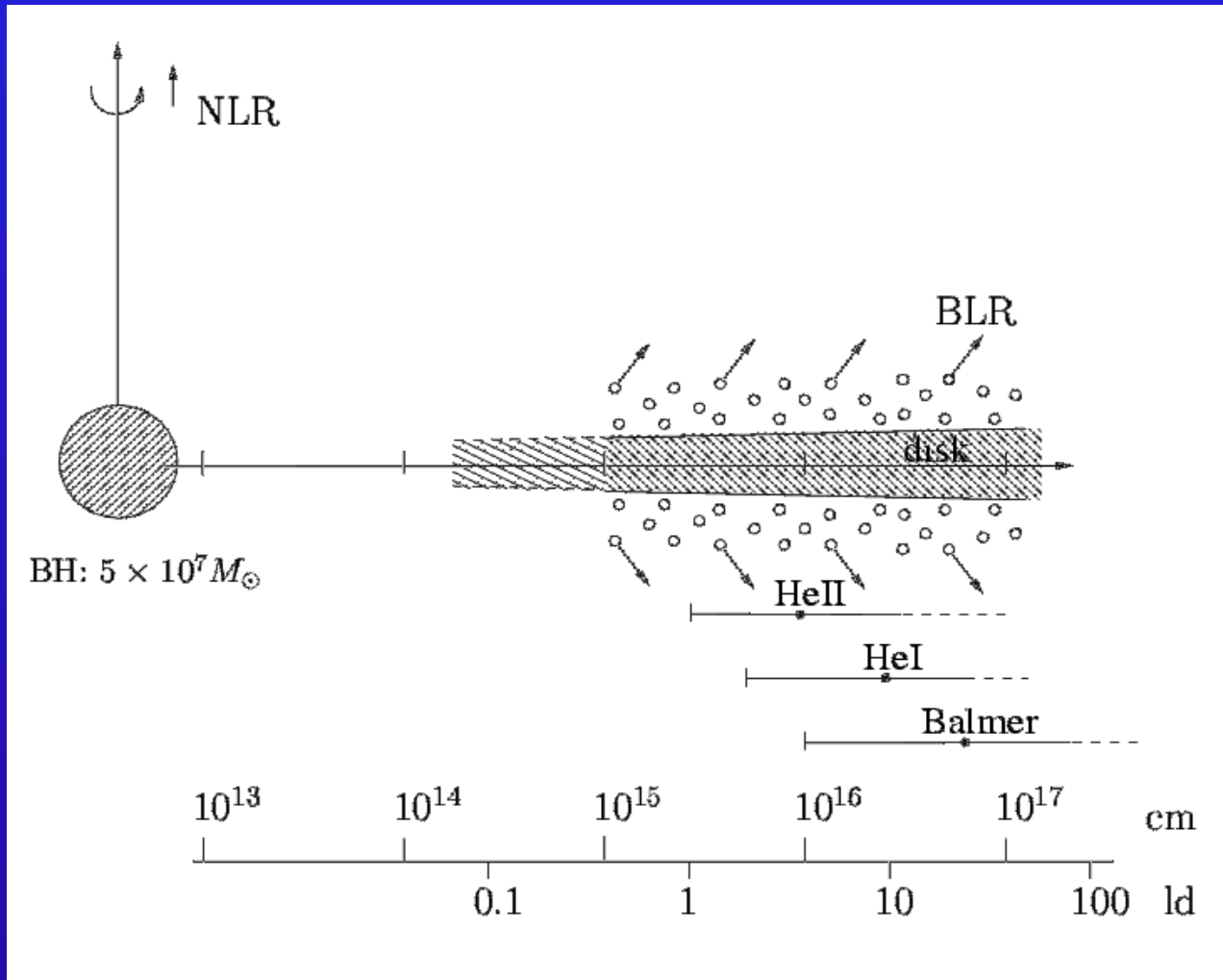


FIG. 13.—Schematic representation of how a disk-driven hydromagnetic wind, which is characterized by a highly stratified density distribution, interacts with the active galactic nucleus (AGN) continuum emission. The innermost regions are heated and ionized by the powerful radiation field, with the temperature and degree of ionization varying both with distance and with the polar angle, whereas the outer regions (beyond the dust sublimation radius) are cooler and contain dust. The radiation pressure force on the dust causes the outer streamlines to have a larger opening angle.

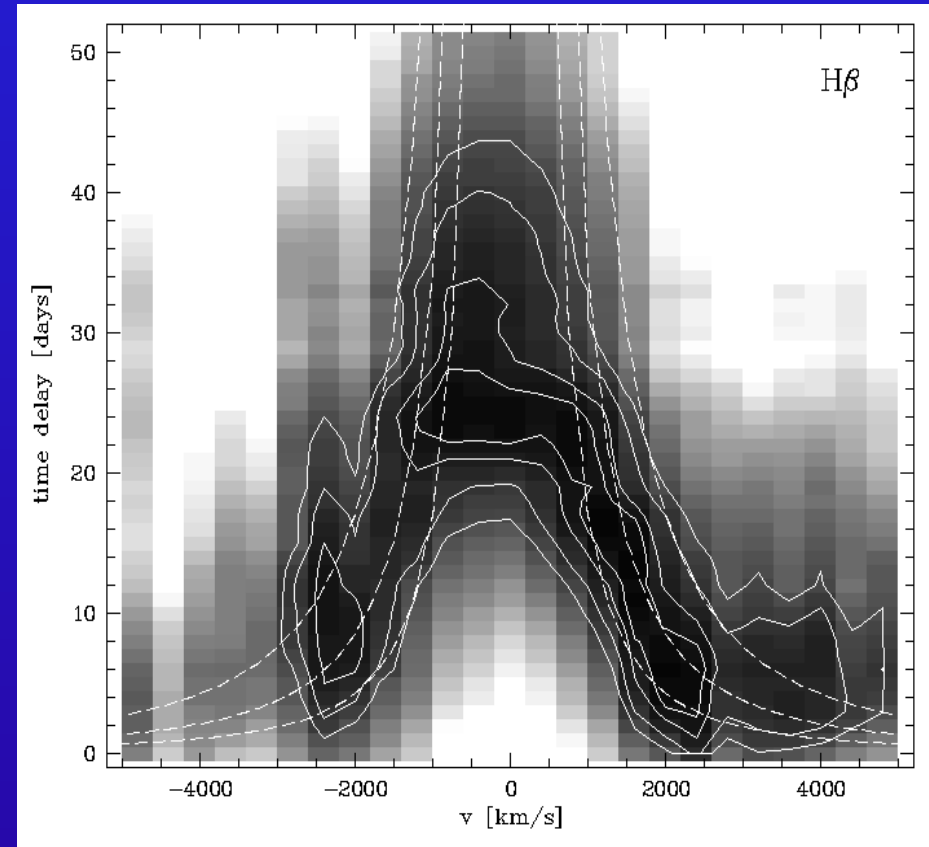
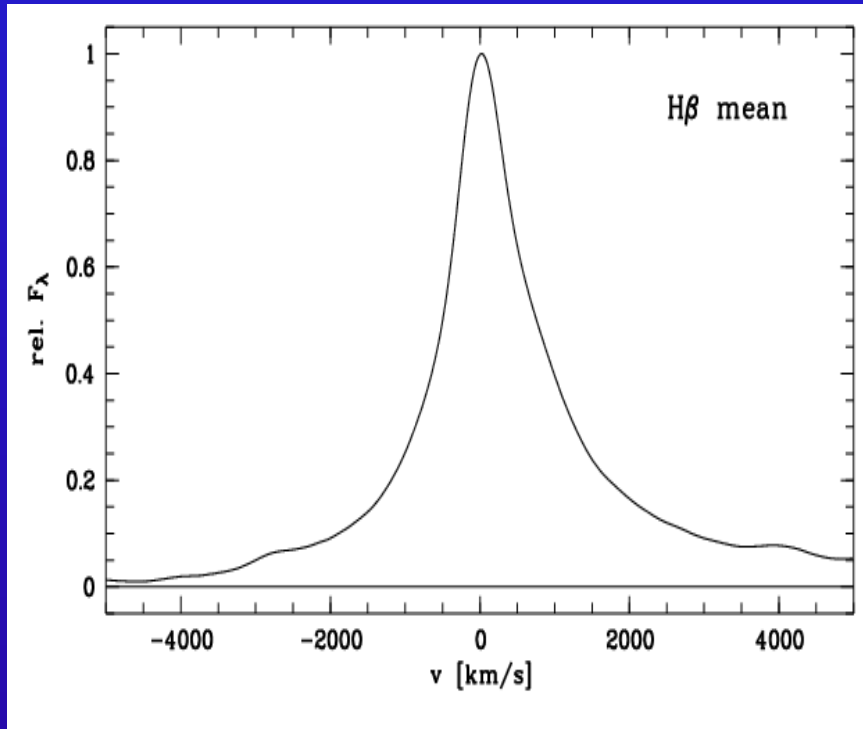
Koenigl & Kartje 1994

accretion disk wind in Mrk110

Kollatschny 2003a

# BLR: Accretion disk structure in Mrk110

*Information about accretion disk structure in Mrk110:  
from line profile variations (not from line profiles)*



Mean H $\beta$  line profile of Mrk110 in  
velocity space

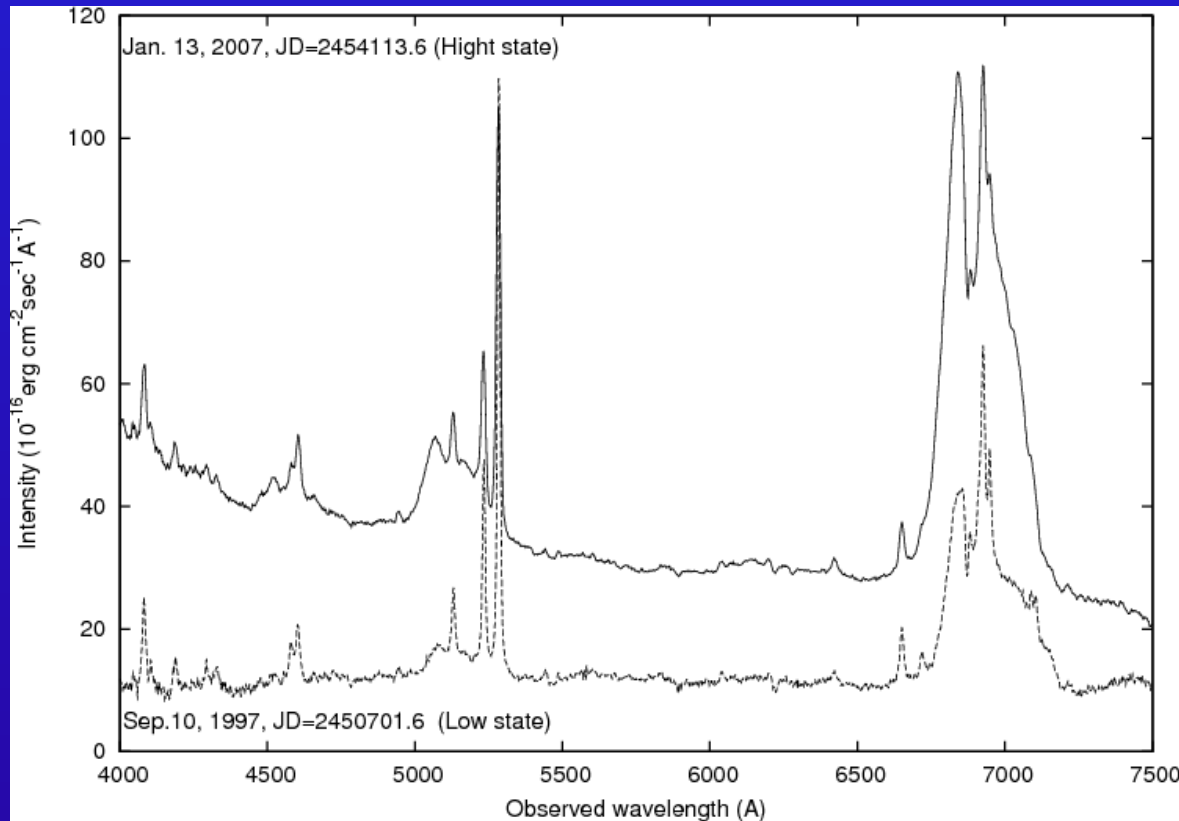
(no indication for accretion disk from line profile)

Velocity-delay map

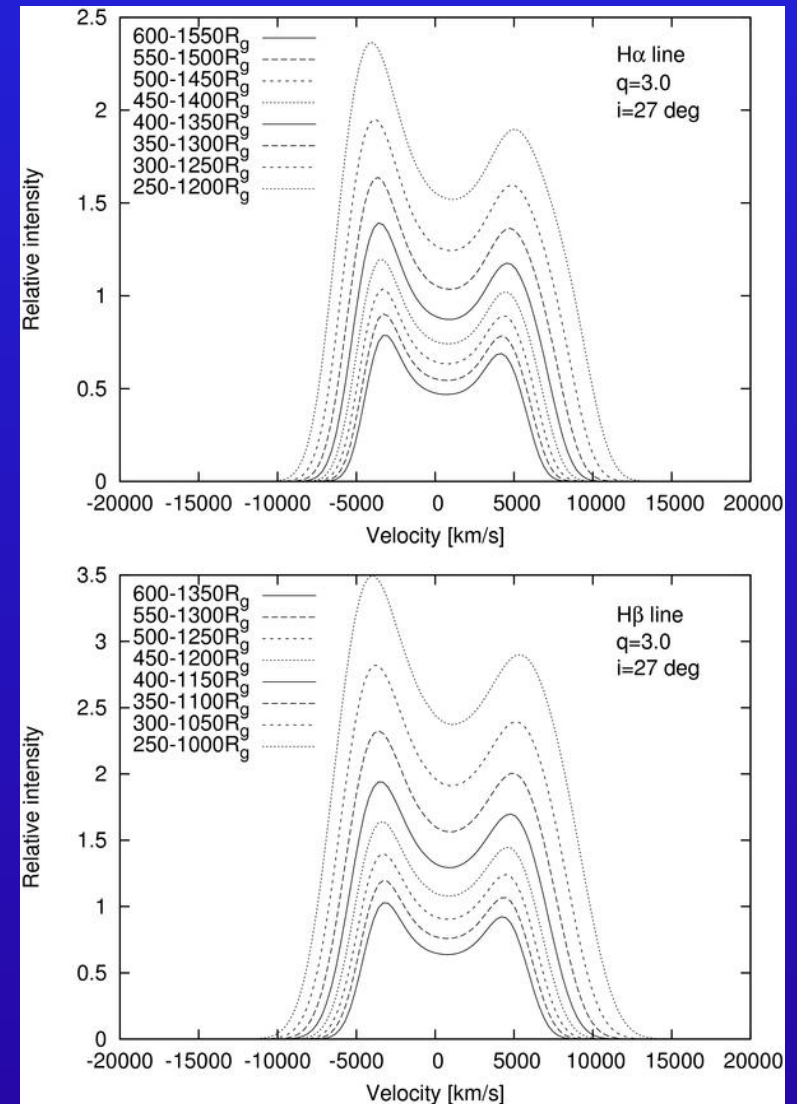
Kollatschny 2003a

# BLR: Accretion disk structure in 3C390.3

Information about accretion disk structure in 3C390.3 from shape of line profiles



Spectra of 3C390.3 close to maximum (2007) and minimum (1997)



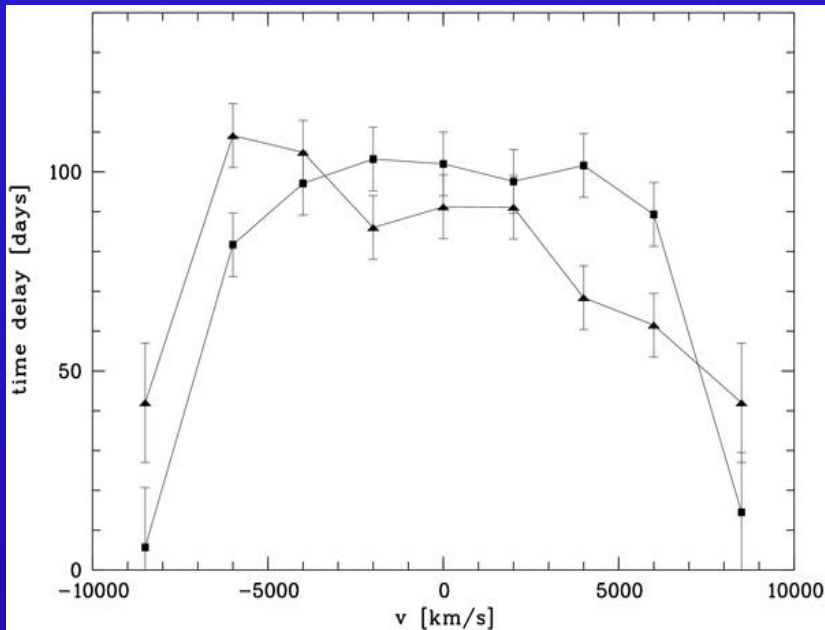
Modeled H $\alpha$ , H $\beta$  line profiles for different disk parameters

Shapovalova et al. 2010, Popovic et al. 2011

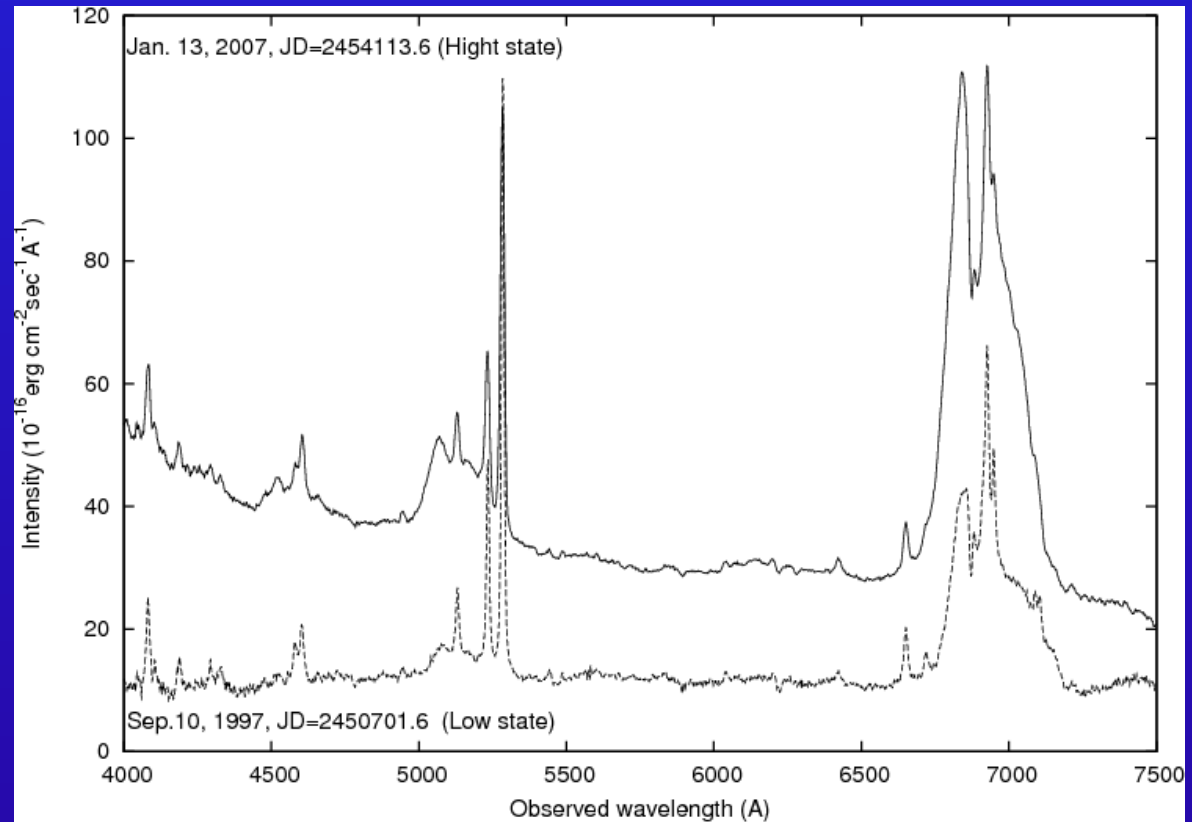


# BLR: Accretion disk structure in 3C390.3

*Information about accretion disk structure in 3C390.3 also from line profile variations*



Time delay of individual H $\beta$  line segments with respect to continuum light curve (1995-2002: squares, 2003-2007: triangles)



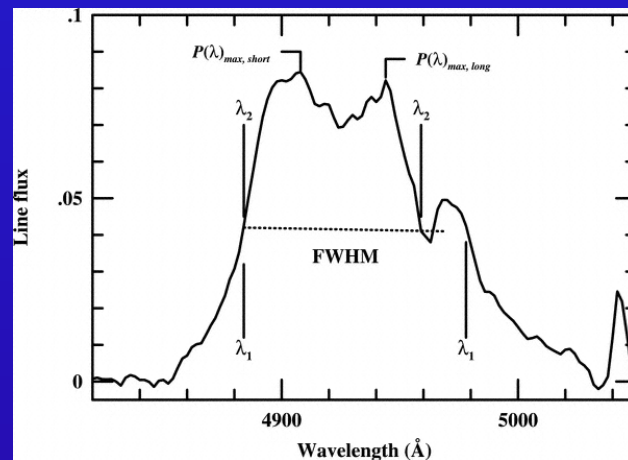
Spectra of 3C390.3 close to maximum (2007) and minimum (1997)

# Line profile studies: BLR structure & kinematics

Black hole mass estimations for 35 AGNs based on improved line-width measurements (*FWHM*, line dispersion  $\sigma$ ) of the mean and rms line profiles of H $\beta$

Given an emission-line profile  $P(\lambda)$  (i.e., flux per unit wavelength above a continuum interpolated underneath the line), we parameterized the line width in two separate ways:

*FWHM*.—How this quantity is measured depends on whether the line is single- or double-peaked. In the case of



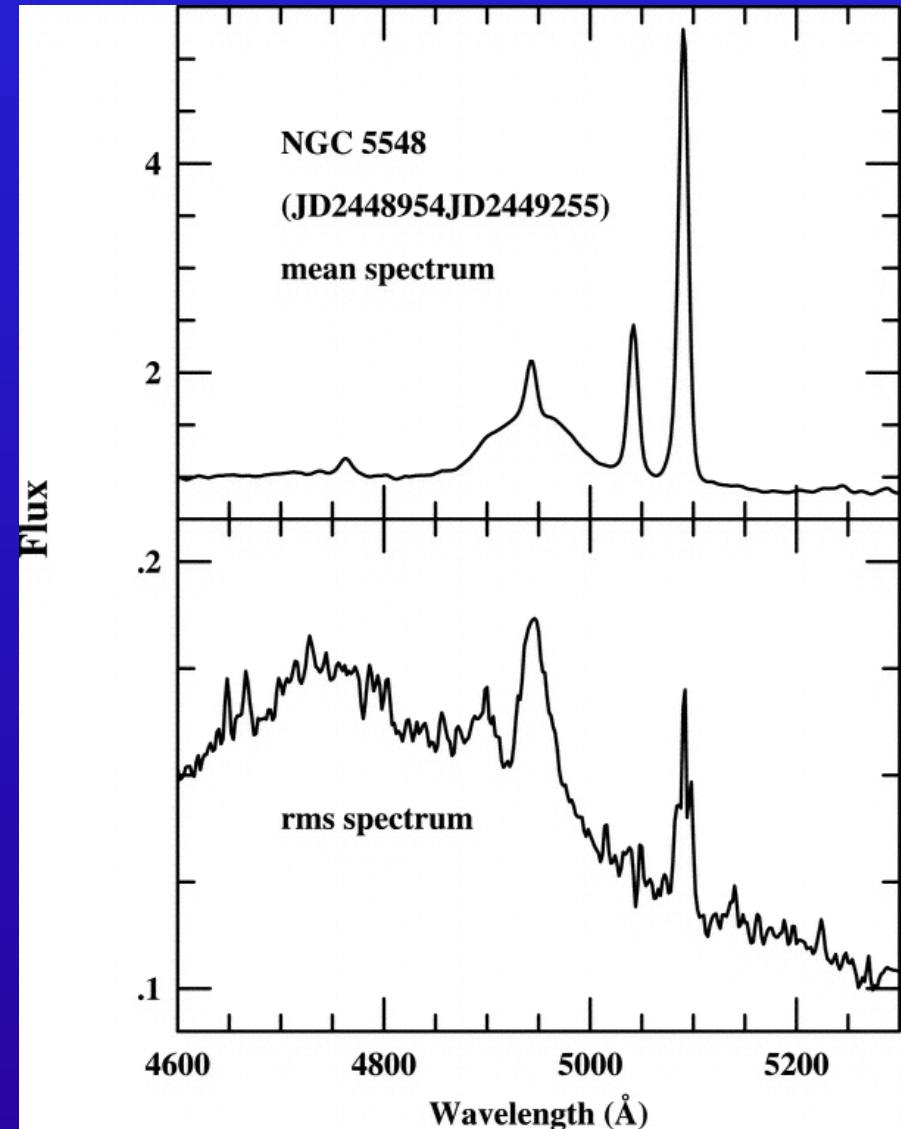
*Line dispersion*.—The first moment of the line profile is

$$\lambda_0 = \int \lambda P(\lambda) d\lambda / \int P(\lambda) d\lambda. \quad (4)$$

We use the second moment of the profile to define the variance or mean square dispersion

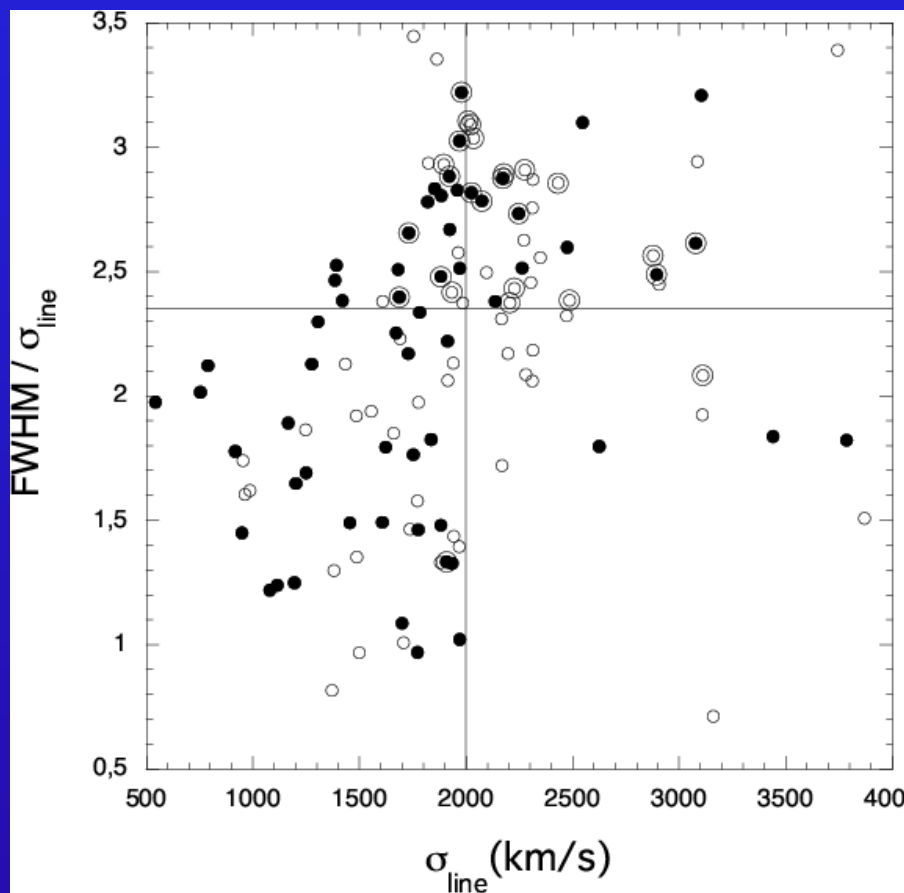
$$\sigma_{\text{line}}^2(\lambda) = \langle \lambda^2 \rangle - \lambda_0^2 = \left[ \int \lambda^2 P(\lambda) d\lambda / \int P(\lambda) d\lambda \right] - \lambda_0^2. \quad (5)$$

The square root of this equation is the line dispersion  $\sigma_{\text{line}}$  or rms width of the line.



Peterson et al., 2004

# H $\beta$ line-width ratio FWHM/ $\sigma$ versus $\sigma$



Peterson, 2004, data set

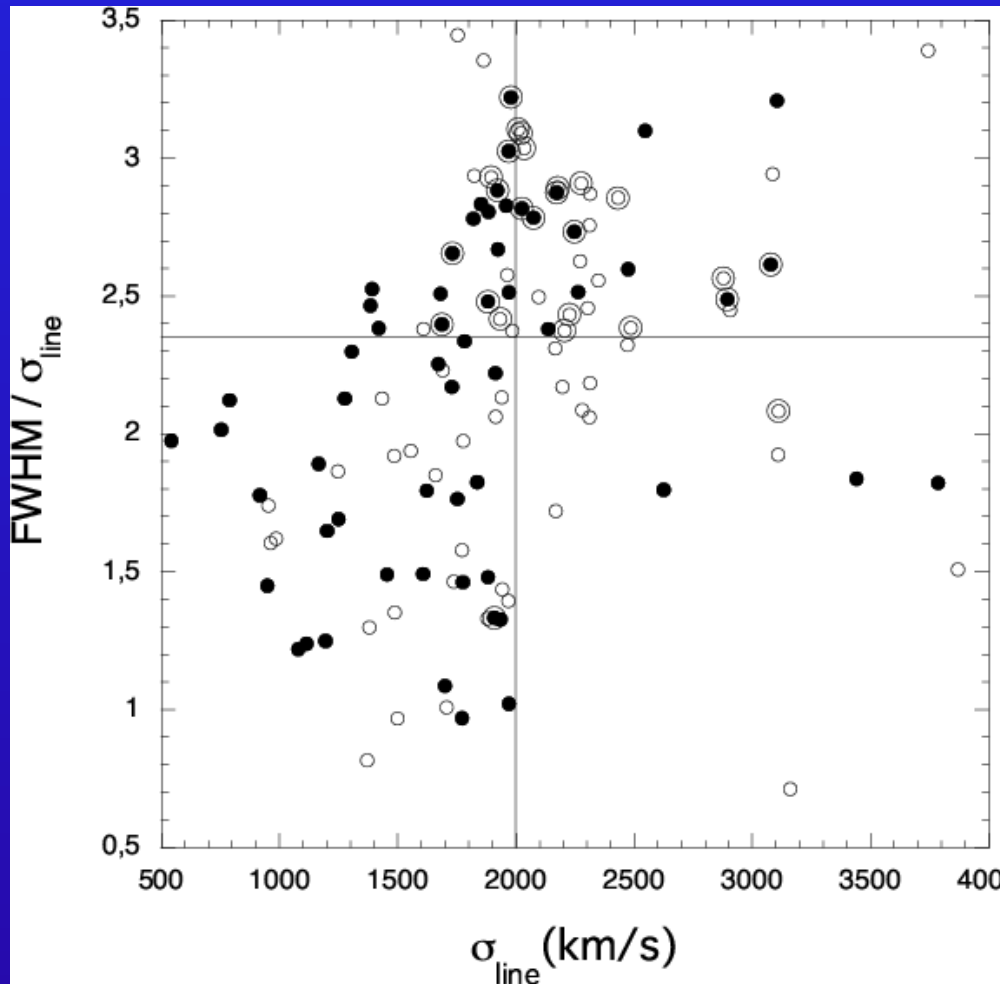
The horizontal line at 2.35 is the value of the ratio for a Gaussian profile.

The open and filled circles correspond respectively to values based on mean and rms spectra.

The vertical line at  $\sigma = 2000$  km/s approximates the division of Sulentic et al. (2000) into Populations A (left) and B (right).

The horizontal line at 2.35 divides the samples into Populations 1 (lower) and 2 (upper) (Collin et al., 2006).

# H $\beta$ line-width ratio FWHM/ $\sigma$ versus $\sigma$



Relationship between FWHM and  $\sigma$  depends on the line profile:

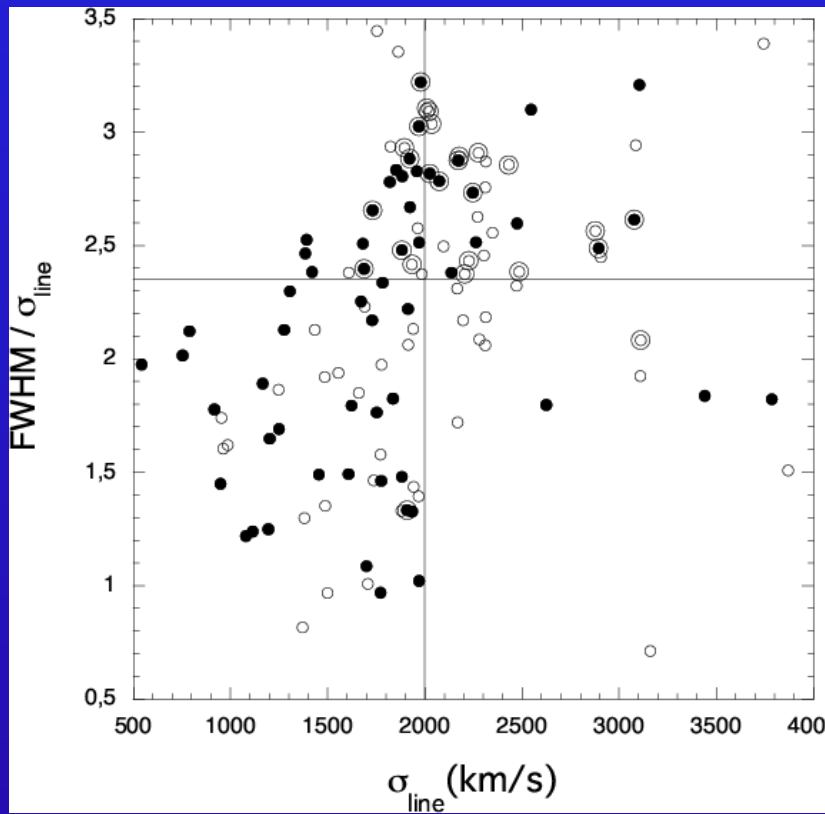
- |                       | FWHM/ $\sigma$    |
|-----------------------|-------------------|
| - rectangular fct.    | 3.46              |
| - edge-on rotat. ring | 2.83              |
| - triangular fct.     | 2.45              |
| - Gaussian profile    | 2.35              |
| - Lorentzian profile  | $\rightarrow 0$ . |

The H $\beta$  line-width ratio FWHM/ $\sigma$  versus  $\sigma$  (mean & rms spectra).

Collin et al., 2006

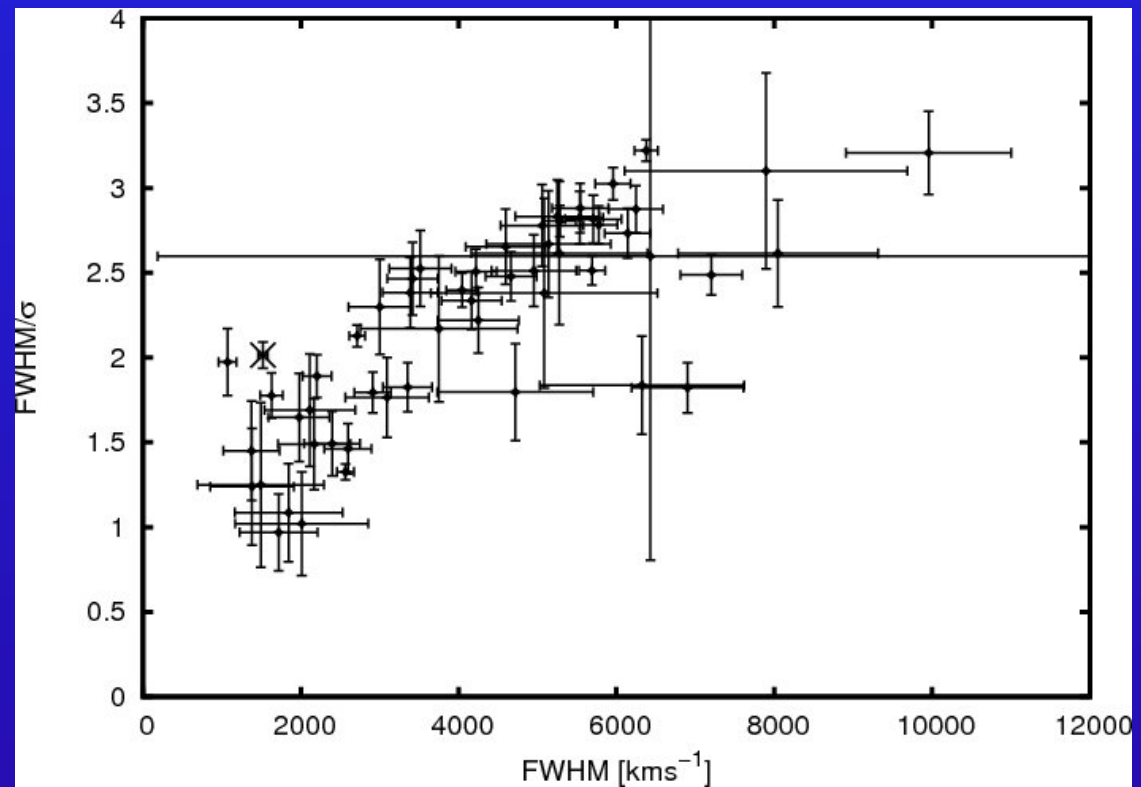
# H $\beta$ line-width ratio FWHM/ $\sigma$ versus $\sigma$ as well as FWHM

Peterson et al., 2004, data set



The H $\beta$  line-width ratio FWHM/ $\sigma$  versus  $\sigma$  (mean & rms profiles).

Collin et al., 2006



The H $\beta$  line-width ratio FWHM/ $\sigma$  versus FWHM (rms profiles) – more continuous.

Mean profiles contaminated by narrow line components.

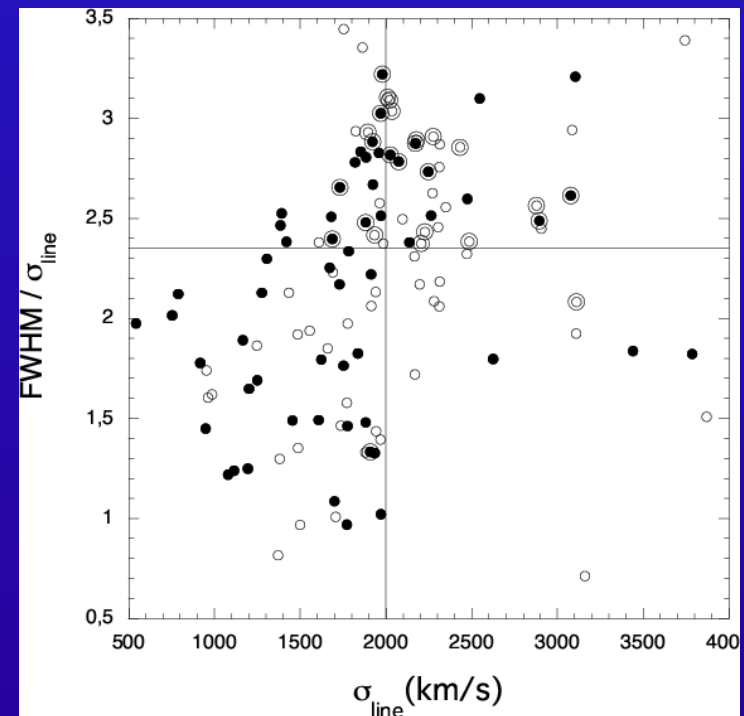
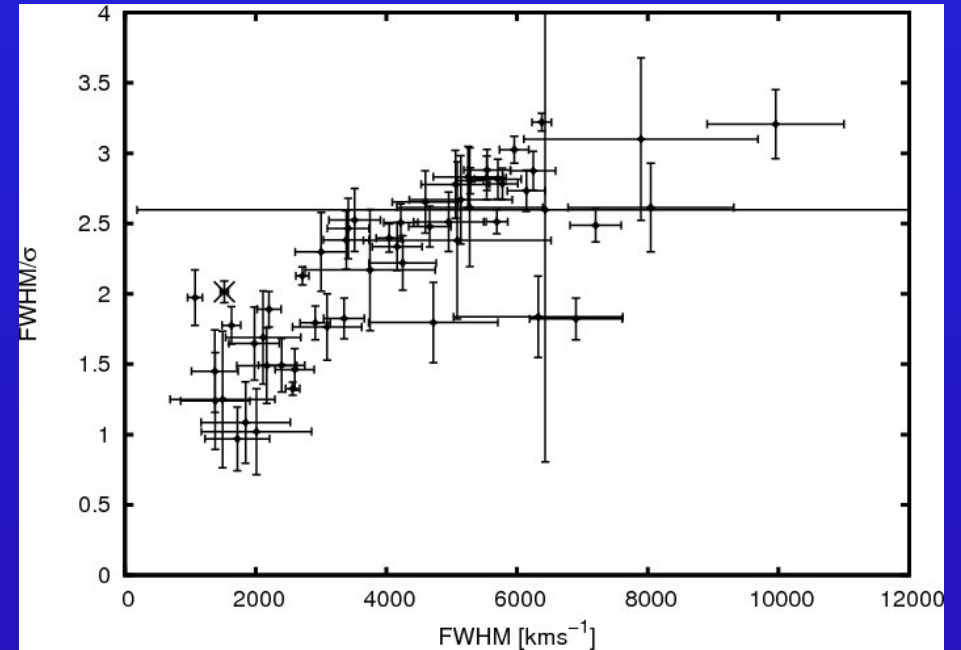
Kollatschny & Zetzl, 2011, Nature 470

# H $\beta$ line-width ratio FWHM/ $\sigma$ versus $\sigma$ as well as FWHM

**Table 1 | Line profile versus linewidth correlations**

	$r_p$	$r_s$	$r_k$	$P_p$	$P_s$	$P_k$
H $\beta$ FWHM/ $\sigma_{line}$ versus FWHM	0.792	0.823	0.649	$6.4 \times 10^{-15}$	$6.4 \times 10^{-11}$	$3.5 \times 10^{-14}$
H $\beta$ FWHM/ $\sigma_{line}$ versus $\sigma_{line}$	0.364	0.513	0.350	0.003	$4.7 \times 10^{-5}$	$4.4 \times 10^{-5}$
He II FWHM/ $\sigma_{line}$ versus FWHM	0.803	0.786	0.571	0.016	0.041	0.048
He II FWHM/ $\sigma_{line}$ versus $\sigma_{line}$	0.464	0.357	0.214	0.247	0.361	0.458
C IV FWHM/ $\sigma_{line}$ versus FWHM	0.821	0.821	0.619	0.023	0.049	0.051
C IV FWHM/ $\sigma_{line}$ versus $\sigma_{line}$	0.599	0.643	0.429	0.155	0.126	0.176

Given are the Pearson correlation coefficient  $r_p$ , the Spearman's rank-correlation coefficient  $r_s$ , as well as the Kendall correlation coefficient  $r_k$  for H $\beta$ , He II  $\lambda = 4,686 \text{ \AA}$  and C IV  $\lambda = 1,550 \text{ \AA}$  linewidth ratios FWHM/ $\sigma_{line}$  versus FWHM as well as FWHM/ $\sigma_{line}$  versus  $\sigma_{line}$ .  $P_p$ ,  $P_s$  and  $P_k$  are the associated percentage probabilities for random correlations<sup>15,16</sup>. The Pearson correlation coefficient tests a linear relation only, while the other correlation coefficients test for a general monotonic relation.

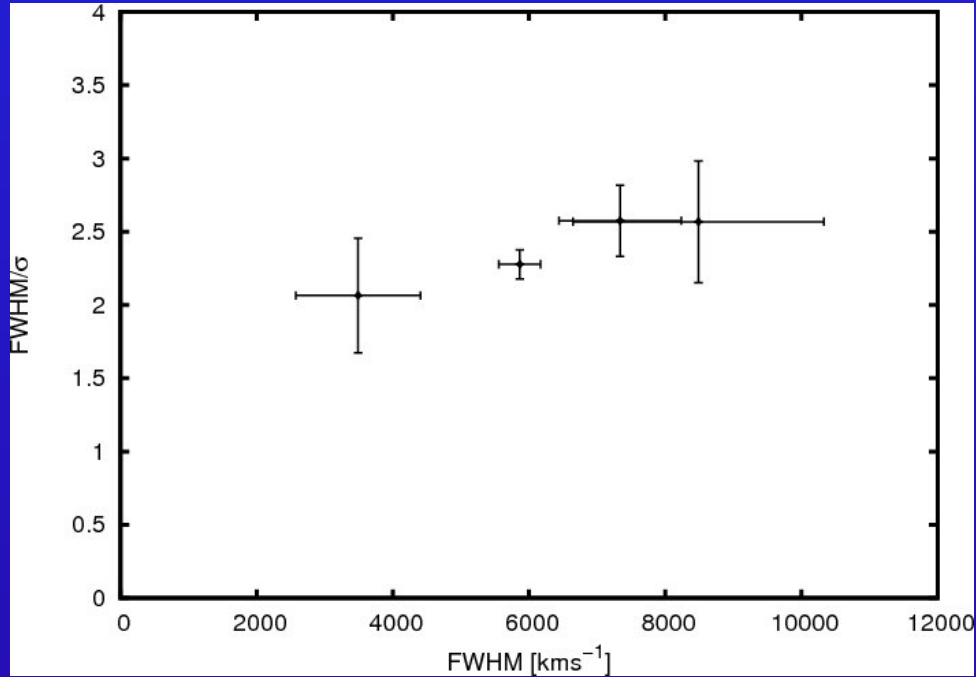


Line profile FWHM/ $\sigma$  versus linewidth (FWHM as well as  $\sigma$ ) correlations.

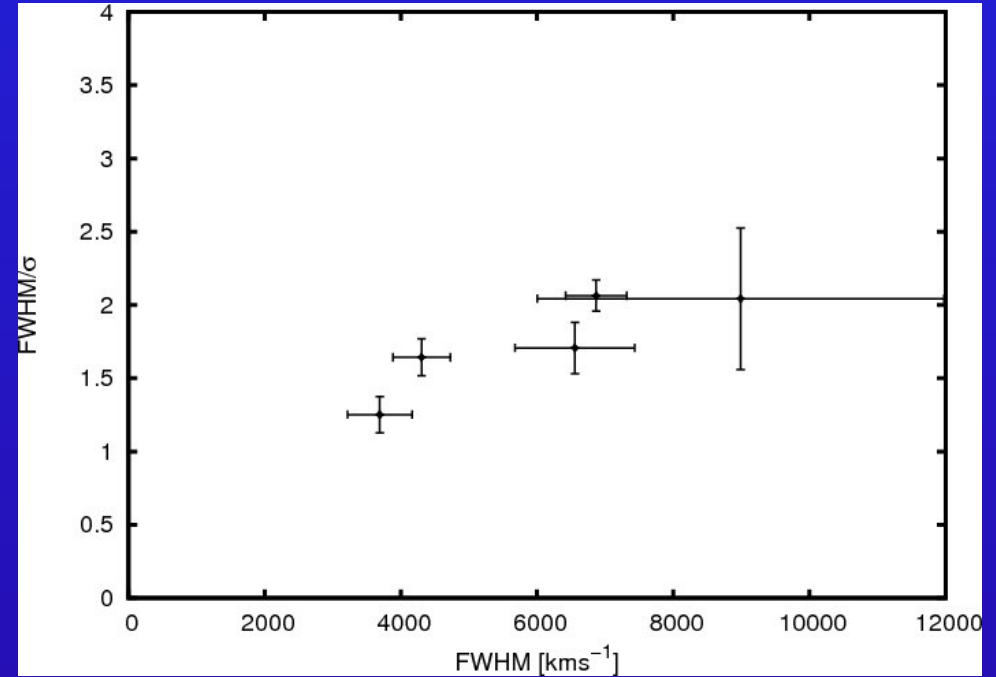
Kollatschny & Zetzl, 2011, Nature 470

# HeII and CIV line-width ratios $\text{FWHM}/\sigma$ versus FWHM

Peterson, 2004, data set:



The HeII  $\lambda 4686$  line-width ratio  $\text{FWHM}/\sigma$  versus FWHM (rms profiles).



The CIV  $\lambda 1550$  line-width ratio  $\text{FWHM}/\sigma$  versus FWHM (rms profiles).

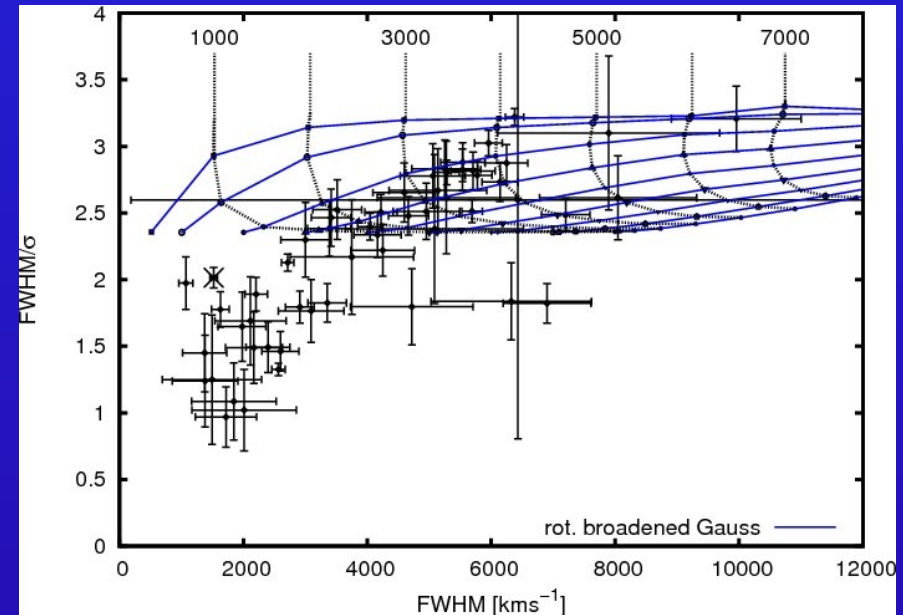
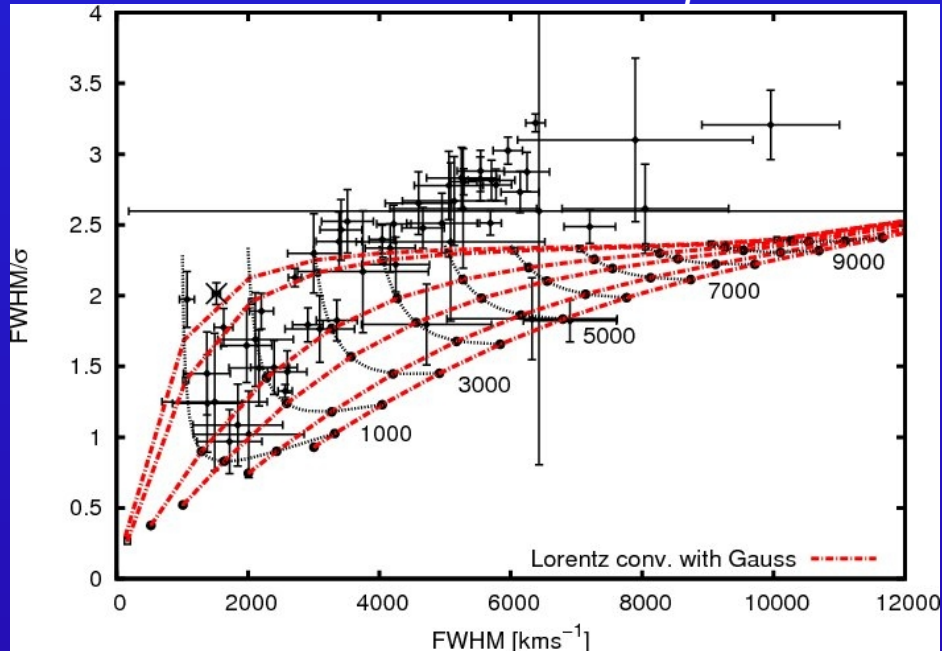
Kollatschny & Zetzl, 2011, Nature 470

*Different emission lines show similar – however unequal – line profile relations.*

# Modeling of observed line profile relations

in simple way by multiple combinations of profiles.

*Observed and theoretical H $\beta$  line-width ratios  $FWHM/\sigma$  versus  $FWHM$*



**Lorentzian profiles convolved with Gaussian profiles.**

The line widths of the Lorentzian profiles ( $FWHM$ ) correspond to 50, 100, 500, 1000, 2000, 3000  $\text{km/s}$  (from top to bottom). The widths of the Gaussian profiles correspond to 1000 to 9000  $\text{km/s}$  (from left to right).

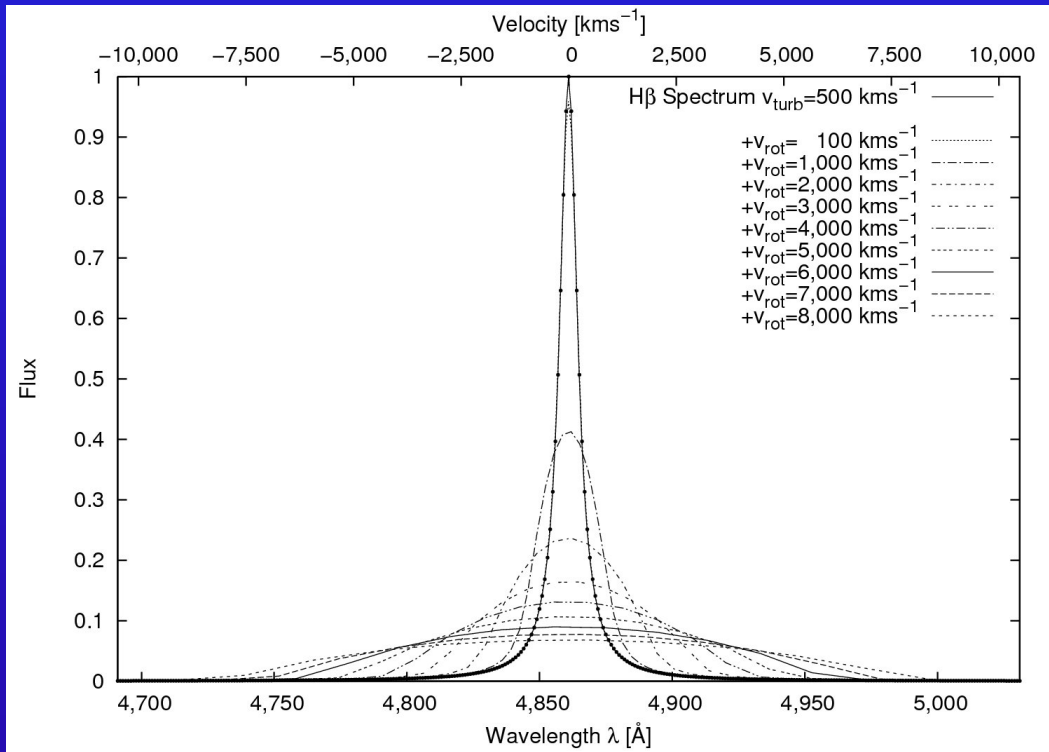
**Rotational broadening of Gaussian profiles.**

The line widths of the Gaussian profiles ( $FWHM$ ) correspond to 500, 1000, ..., 8000  $\text{km/s}$  (from top to bottom). The associated rotational velocities range from 1000 to 7000  $\text{km/s}$  (from left to right).  $FWHM/\sigma$  always larger than 2.35.

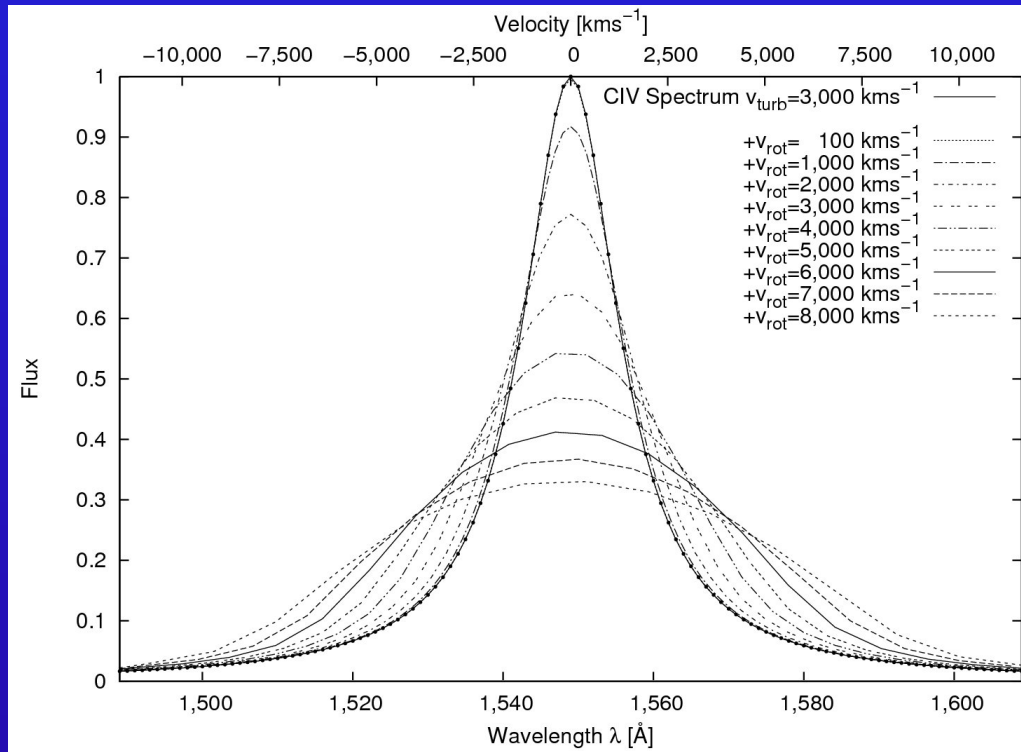


# Modeling of observed line profile relations

Tests: *Theoretical line broadening of Lorentzian profiles due to rotation.*



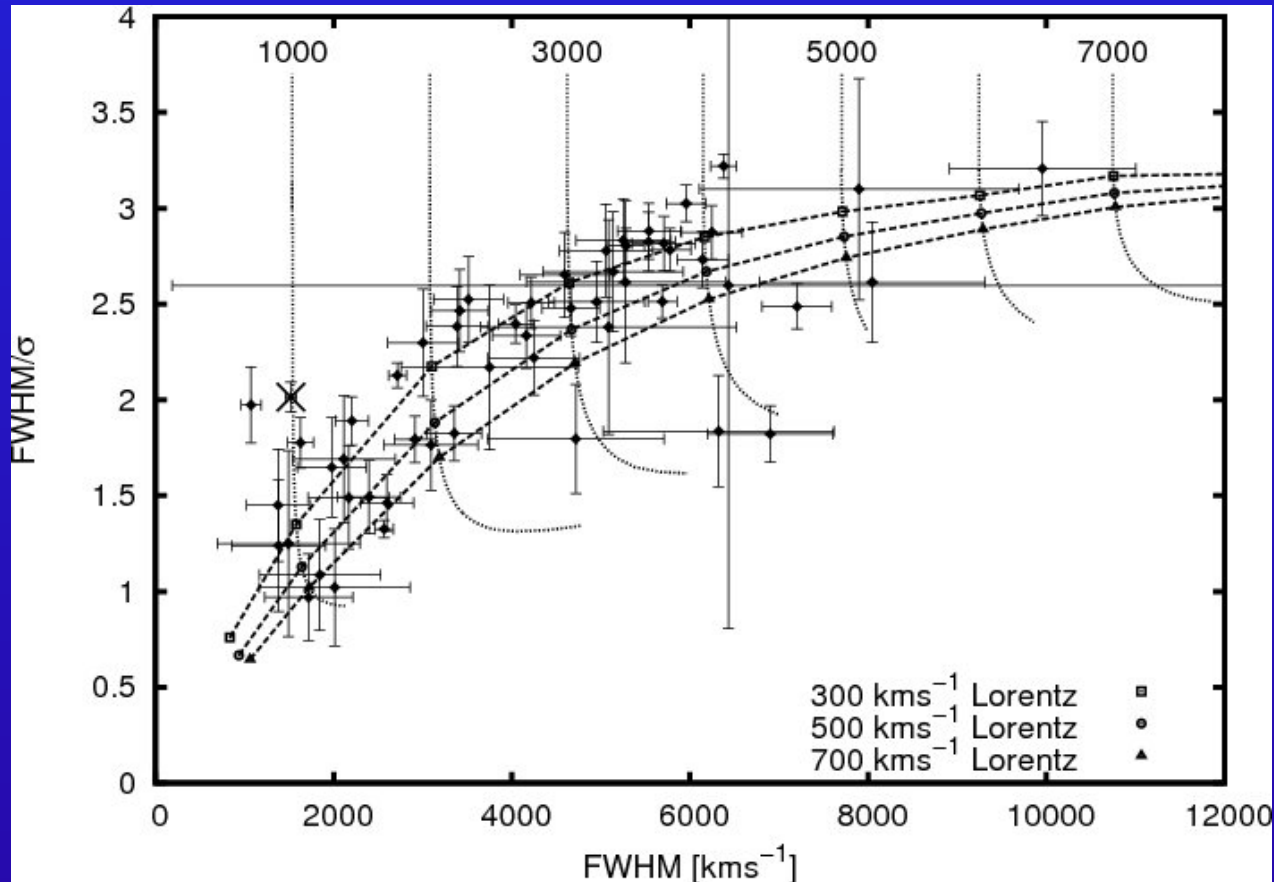
Rotational broadening of Lorentzian H $\beta$  line profile ( $v_{\text{turb}} = 500 \text{ km/s}$ ).



Rotational broadening of Lorentzian CIV $\lambda$ 1550 line profile ( $v_{\text{turb}} = 3000 \text{ km/s}$ ).

# Observed and modeled $H\beta$ line widths ratios

FWHM/ $\sigma$  versus linewidth FWHM

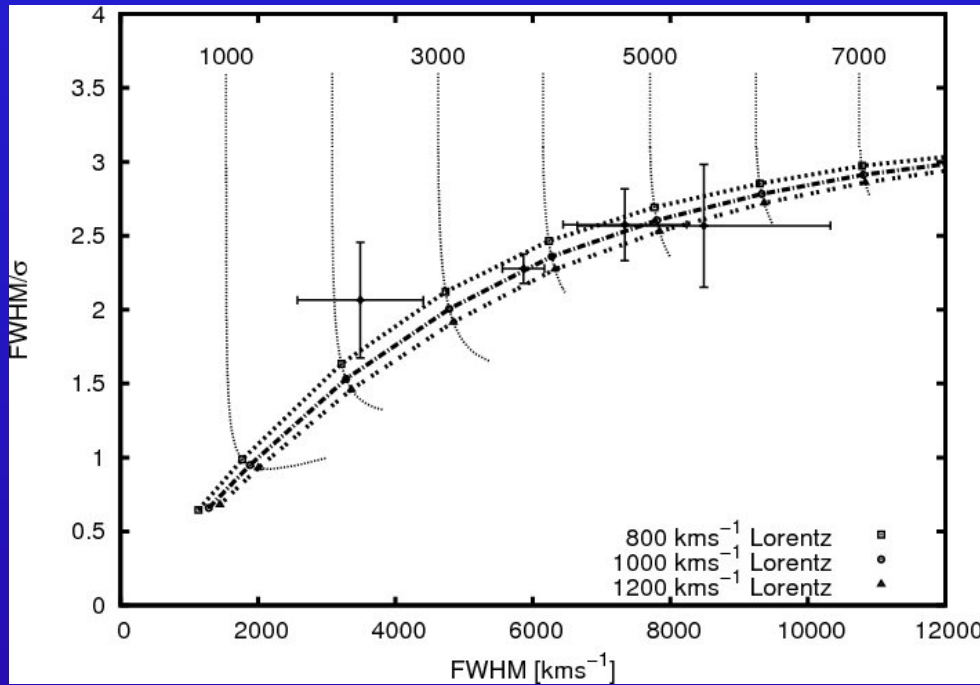


*Dashed curves: rotational line broadened Lorentzian profiles (FWHM = 300, 500, 700 km/s). Rotational velocities range from 1000 to 7000 km/s.*

# Observed and modeled HeII and CIV line widths ratios

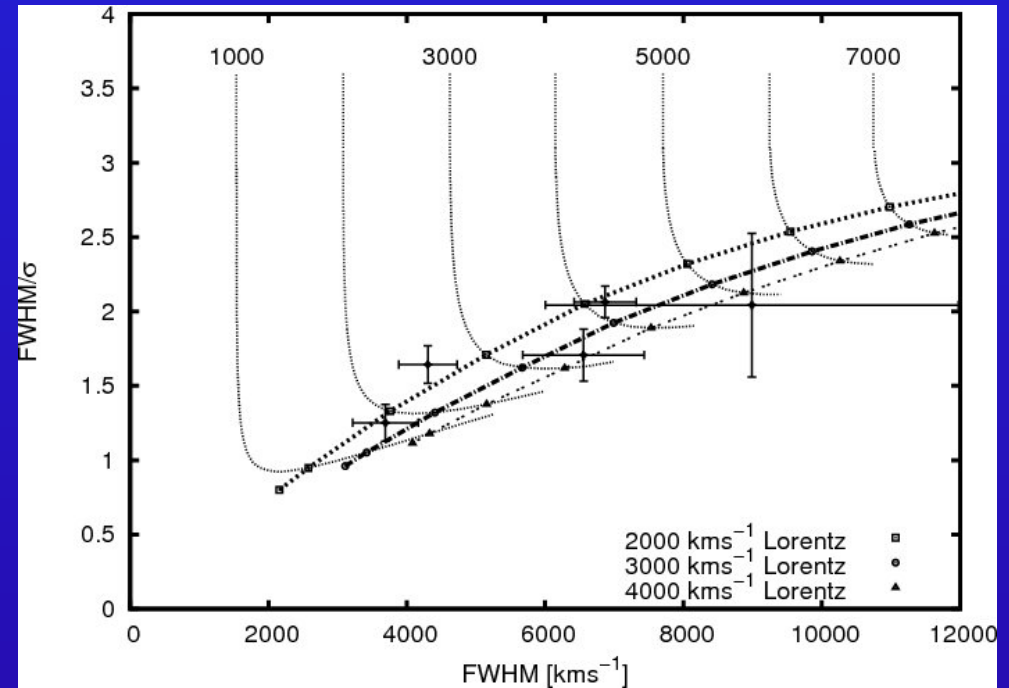
## FWHM/ $\sigma$ versus linewidth FWHM

### HeII $\lambda$ 4686



*Dashed curves: theoretical linewidth ratios of rotational line broadened Lorentzian profiles (FWHM = 800, 1000, 1200 km/s). Rotational velocities range from 1000 to 7000 km/s.*

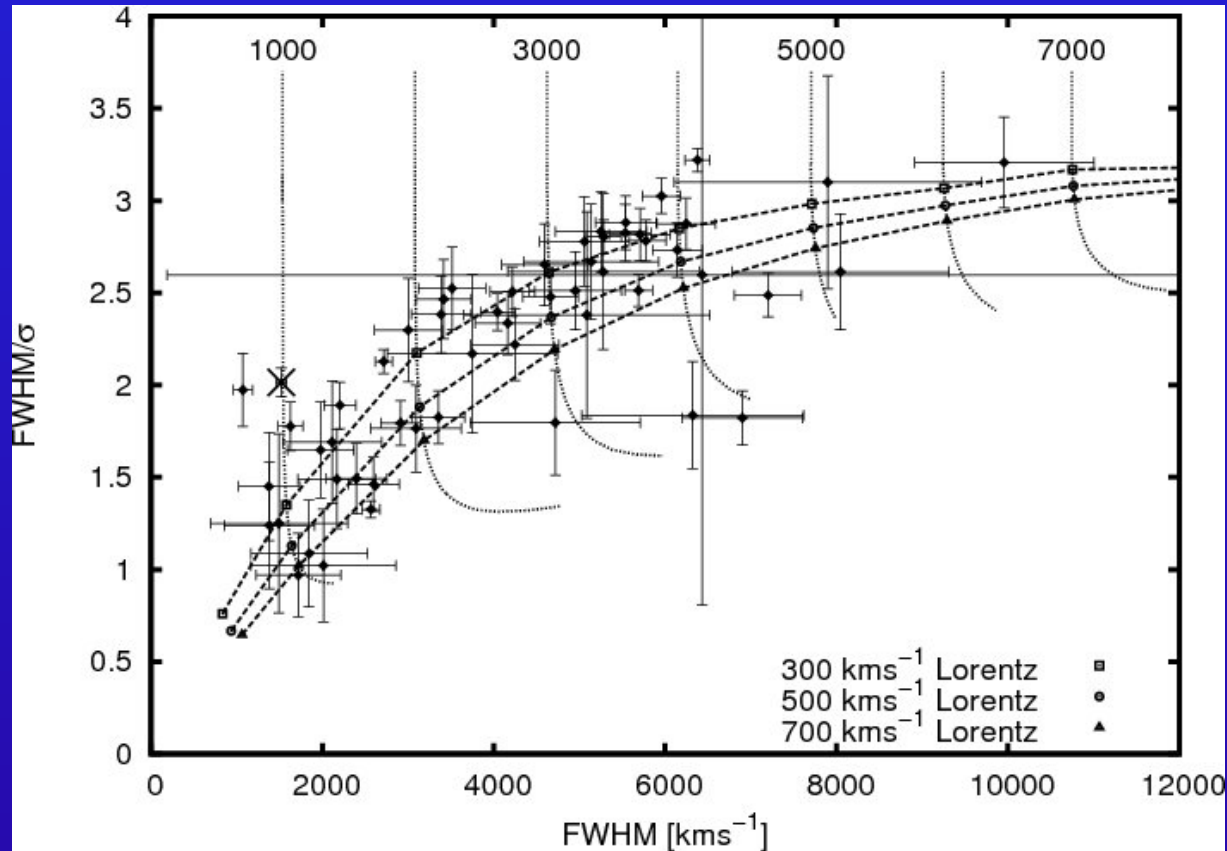
### CIV $\lambda$ 1550



*Dashed curves: theoretical linewidth ratios of rotational line broadened Lorentzian profiles (FWHM = 2000, 3000, 4000 km/s). Rotational velocities range from 1000 to 7000 km/s.*

# Line profile studies: BLR structure & kinematics

Observed and modeled  $H\beta$  line-width ratios  $FWHM/\sigma$  versus linewidth FWHM.



Deviations from general trend: by e.g. orientation effects of line-emitting accretion disk: *an inclined accretion disk leads to smaller linewidths owing to projection effects while the  $FWHM/\sigma$  remains constant (e.g. Mrk110 marked by a cross ( $i \sim 21^\circ$ )).*

# Line profile studies: BLR structure & kinematics

Characteristic turbulent velocities belong to individual emission lines in BLR of all AGN:

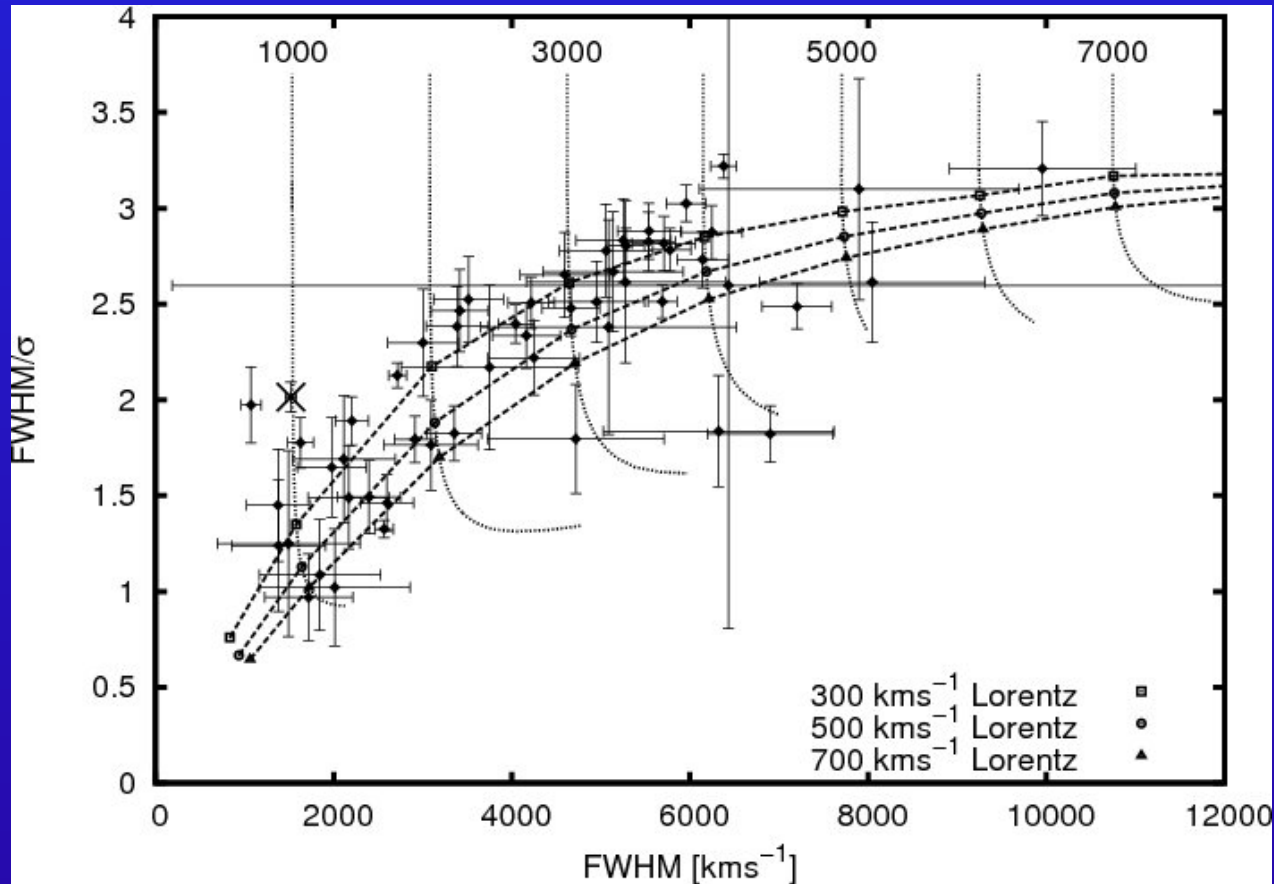
- $H\beta$  :  $500 \pm 200$  km/s
- $HeII\lambda 4686$  :  $1000 \pm 200$  km/s
- $CIV\lambda 1550$  :  $3000 \pm 1000$  km/s

Individual emission lines originate at different distances from center (rev. mapping): →

Turbulent velocity varies as function of distance to center.

# Observed and modeled $H\beta$ line widths ratios

FWHM/ $\sigma$  versus linewidth FWHM



In **all** AGN:  $H\beta$  turbulent velocity  $\sim 500 \text{ km/s}$

Rotation velocity different in individual galaxies:  $500 - 7000 \text{ km/s}$

# Line profile studies: BLR structure & kinematics

From accretion disk theory (e.g. Pringle, 1981):

$$H(\text{height}) / R(\text{adius}) = 1/\alpha * v_{\text{turb}} / v_{\text{rot}} \quad \alpha = (\text{const.}) \text{ viscosity parameter}$$

→ fast rotating broad line AGN: *geometrically thin accretion disk*

→ slow rotating narrow line AGN: *geometrically thick accretion disk*

Different H $\beta$  line widths → different rotational vel. → different BLR geometries:

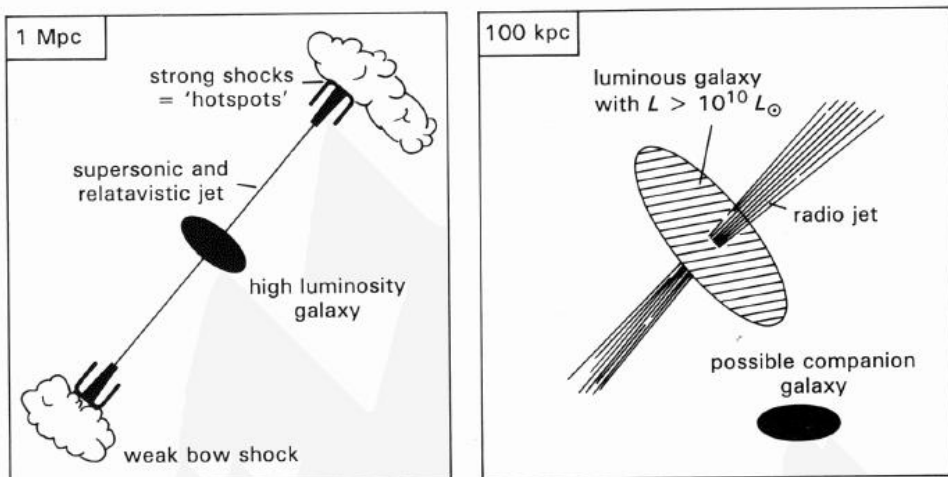
**Eigenvector 1 correlation between linewidth, strong FeII emission, soft X-ray excess:** due to different BLR/disk geometries

Kollatschny & Zetzl, 2011, Nature 470

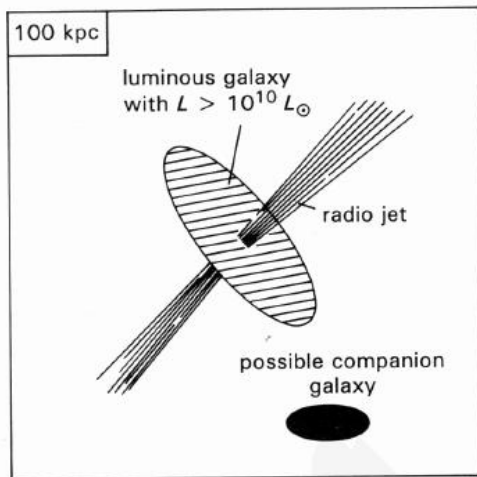




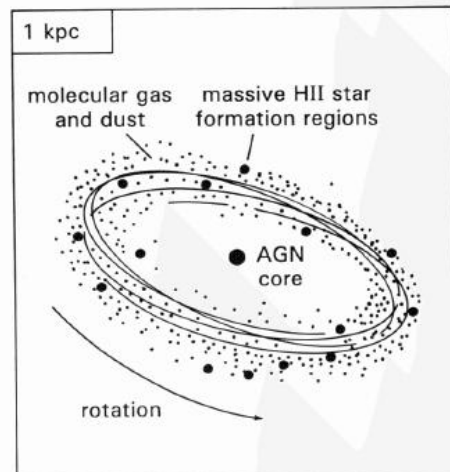
# Scale Sizes of an AGN



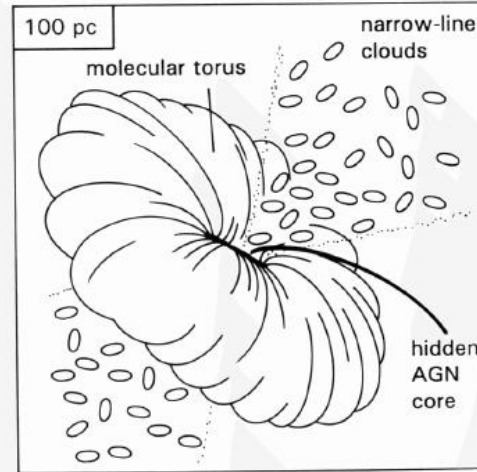
Extended radio sources — shown is an FR II source with an edge-brightened structure. The FRIs have lower jet velocities and fade-out to the ends.



The host galaxy. Although shown as an early type galaxy with a smooth profile, it could also be highly irregular with multiple nuclei as a result of merging.

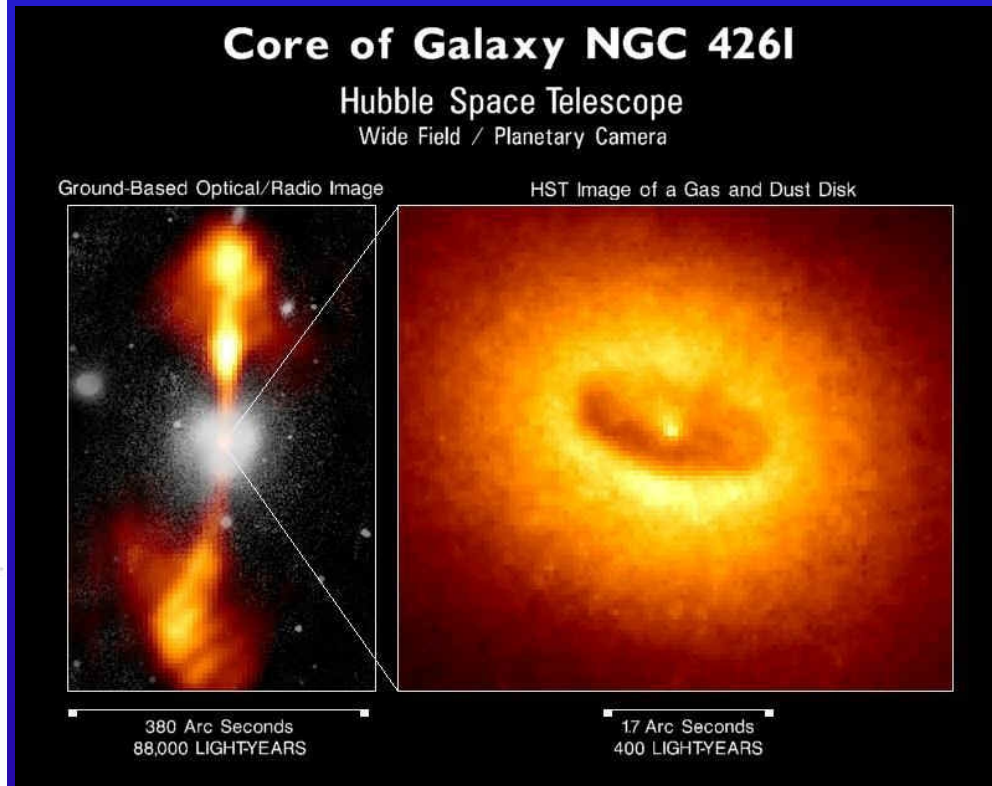


The central kpc star formation disk. This strong far infrared emitting zone might be fed by a bar structure, as seems to be the case for NGC1068.

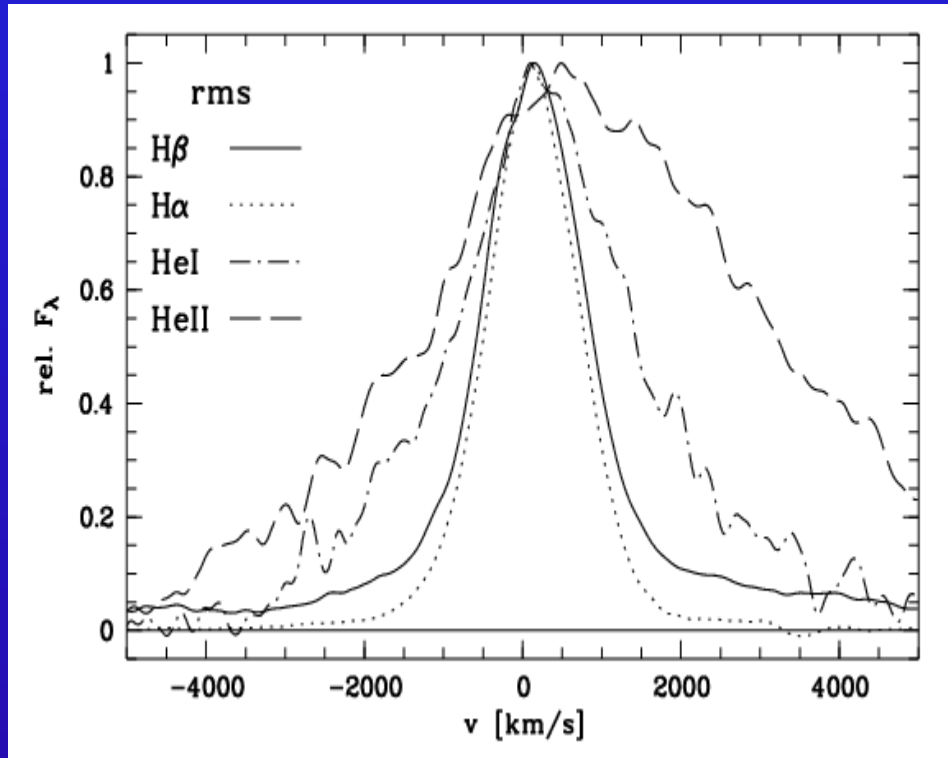


The narrow-line region comprising small but numerous clouds of the interstellar medium ionized by the central AGN core.

Fig. 9.9 Cartoon of the representative scale sizes of an AGN. How we eventually see the object depends on a number of parameters, the main one being the orientation of the obscuring torus with respect to the observer. (Adapted from Blandford, *Active Galactic Nuclei*, Saas-Fee Advanced Course 20, Springer-Verlag, 1990.)

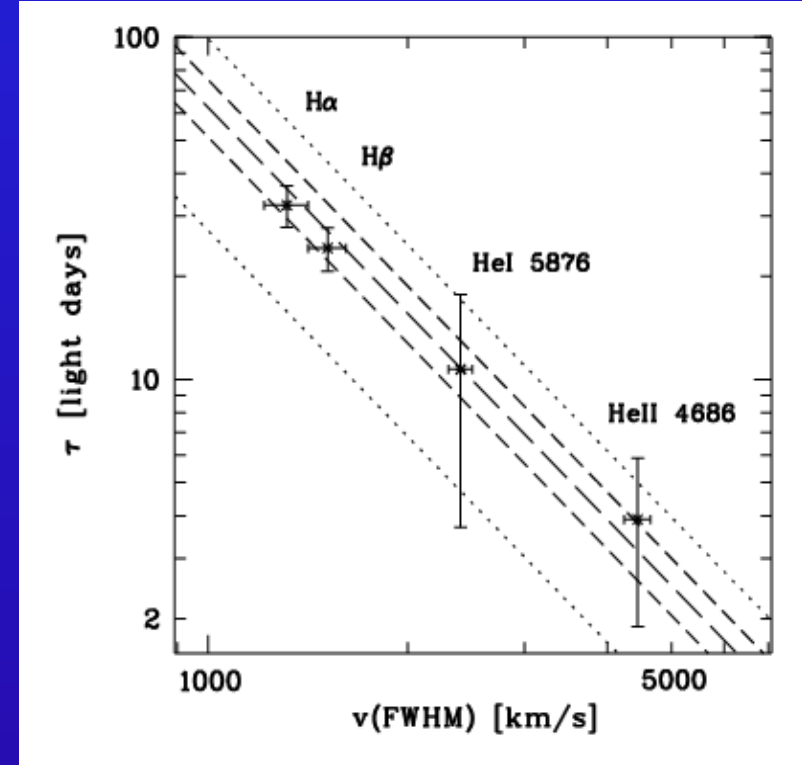


# BLR size and stratification in Mrk110



Normalized rms line profiles in velocity space

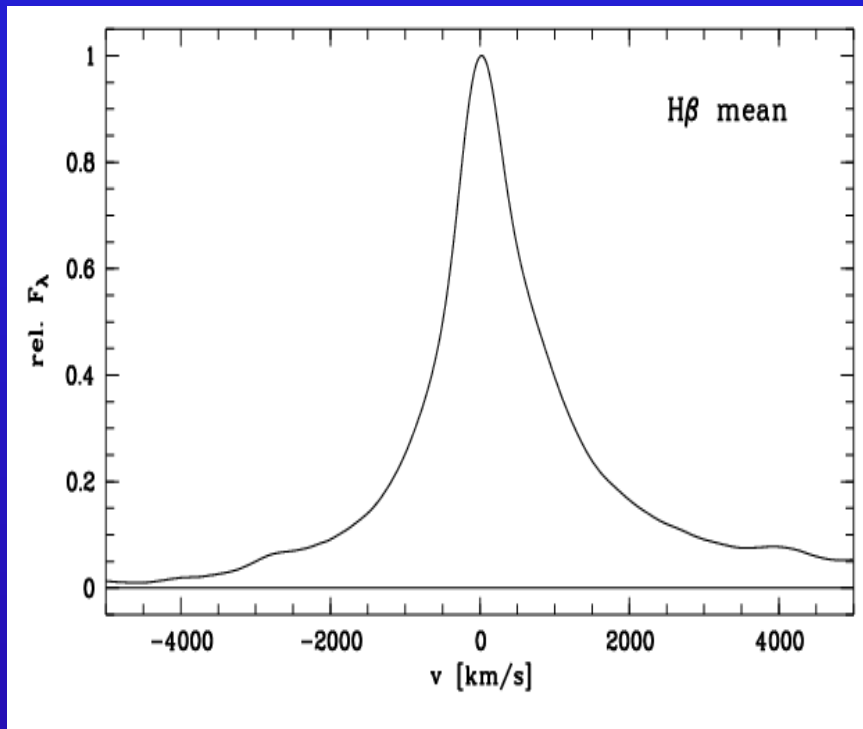
The rms spectrum shows the variable part of the spectrum



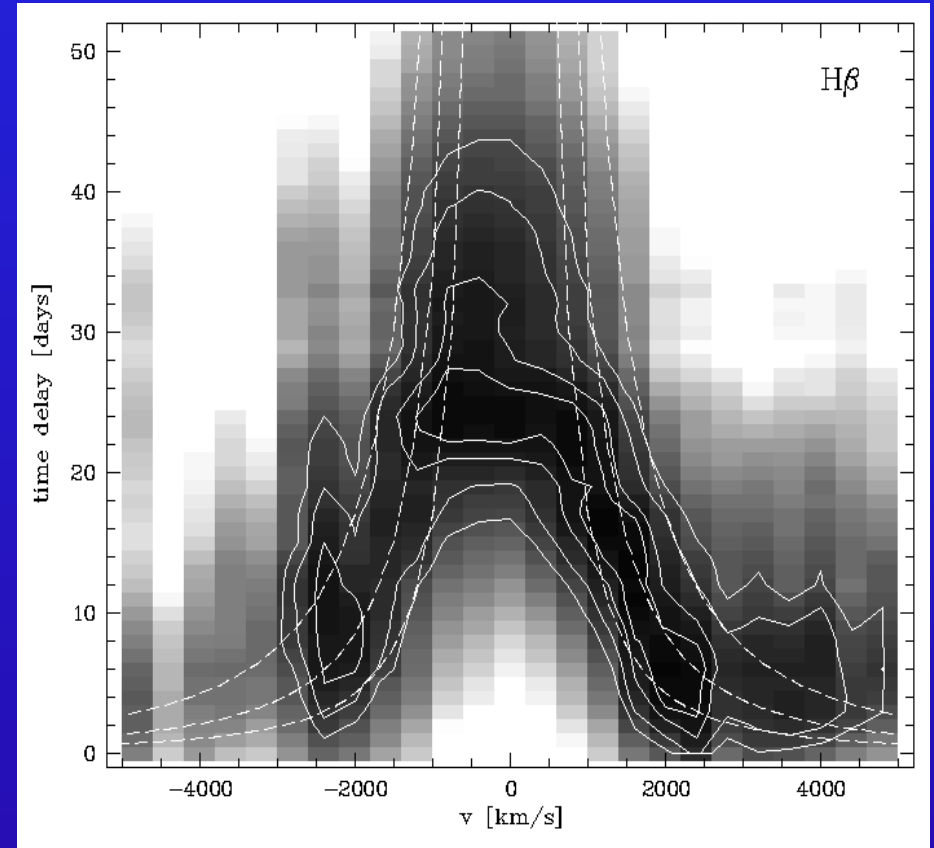
Mean distances of the line emitting regions from central ionizing source as function of FWHM in rms profiles.

The dotted and dashed lines correspond to virial masses of  $.8 - 2.9 \cdot 10^7 M_\odot$  (from bottom to top).

# BLR: Accretion disk structure in Mrk110



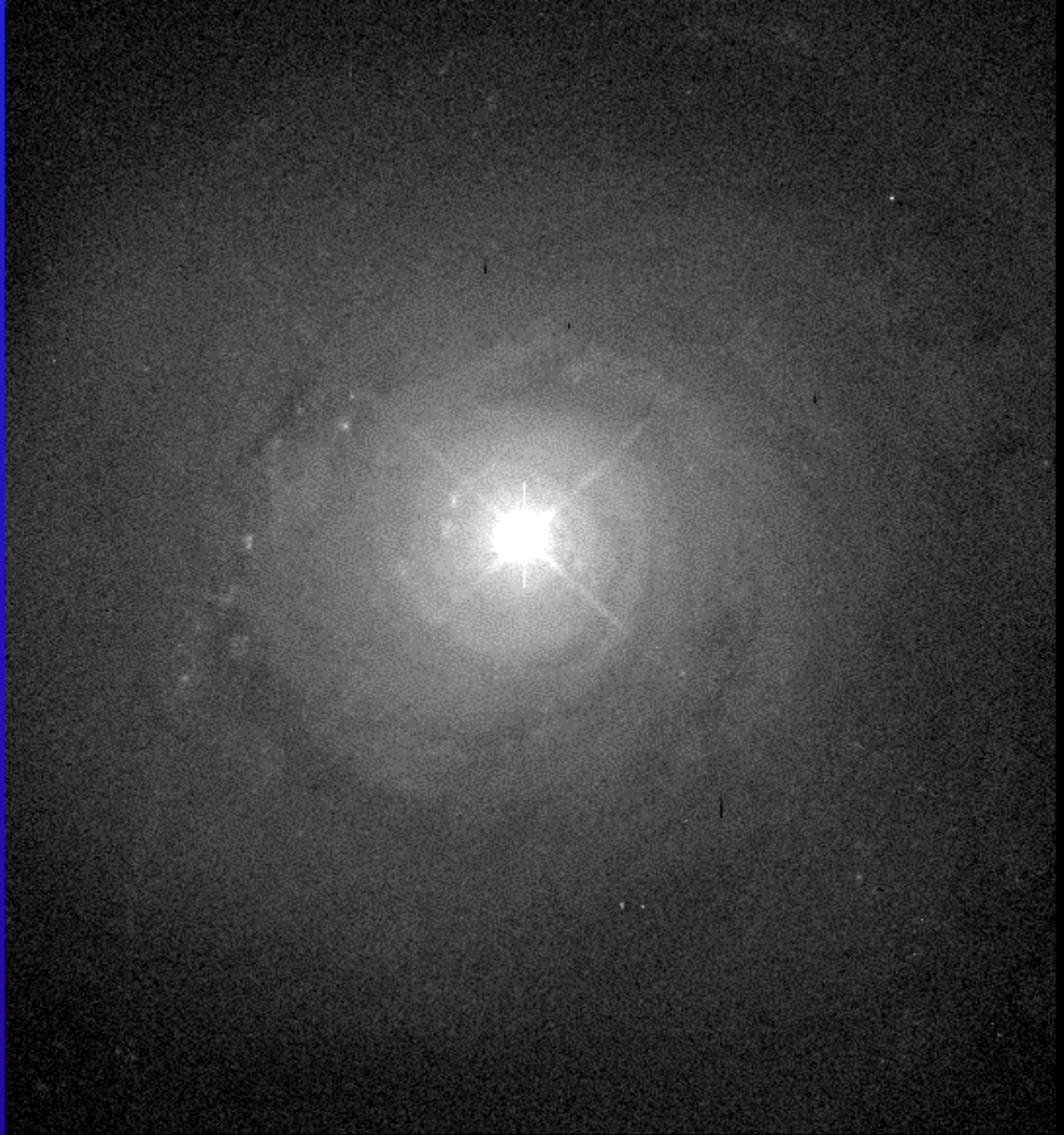
Mean H $\beta$  line profile of Mrk110  
in velocity space



Velocity-delay map

Kollatschny 2003a

# HST Image of NGC5548



NGC5548

$V = 13.7$

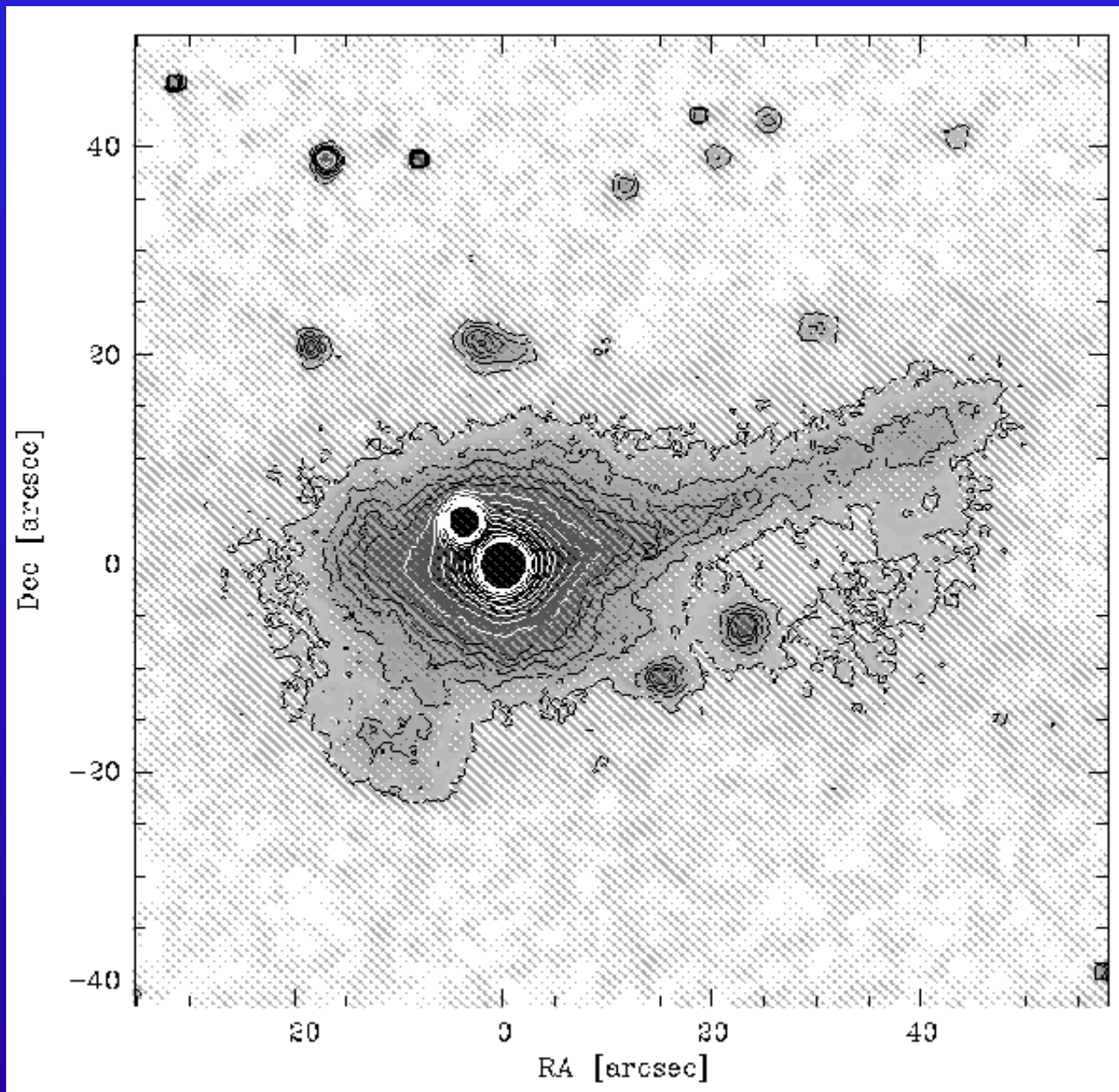
$M_V = -20.7$

$z = 0.017$

$\text{FWHM}(H\beta) = 4400 \text{ km s}^{-1}$

25 x 30 arcsec

# BLR size and stratification in Mrk110



Mrk110

$V = 15.4$

$M_V = -20.6$

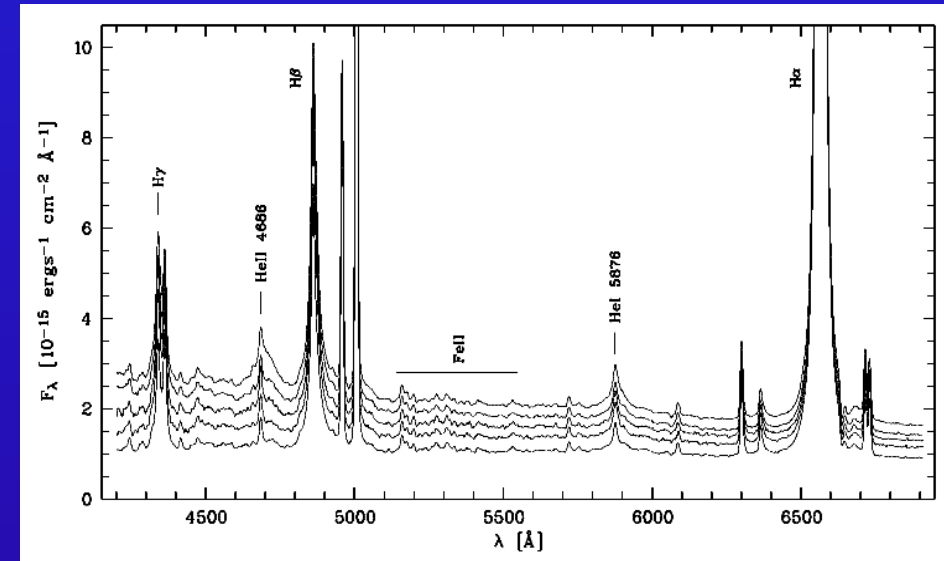
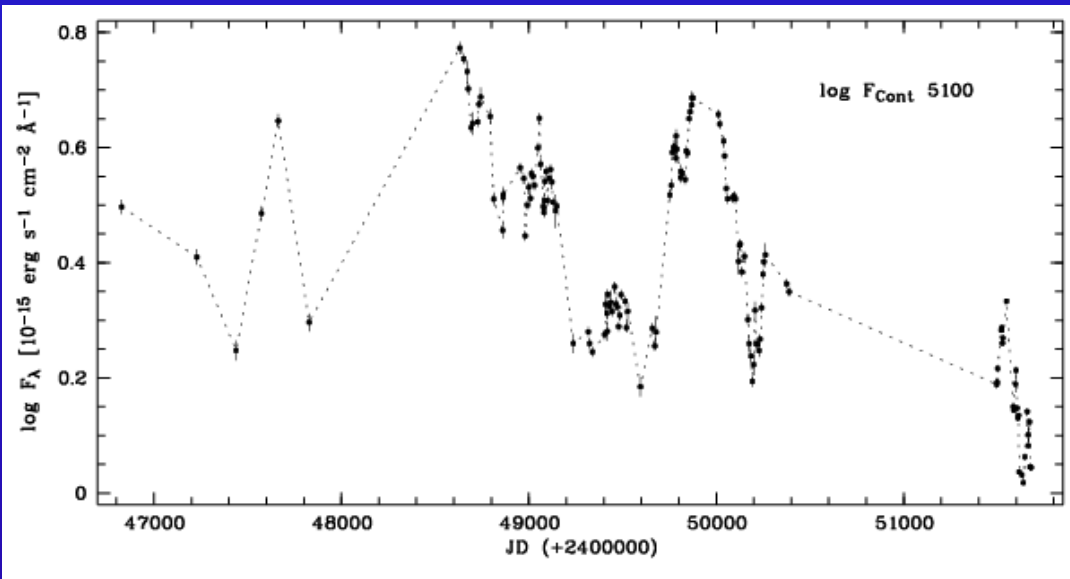
$z = 0.036$

$\text{FWHM}(\text{H}\beta) = 1680 \text{ km s}^{-1}$

tidal arm: 35kpc

# HET variability campaign of Mrk110

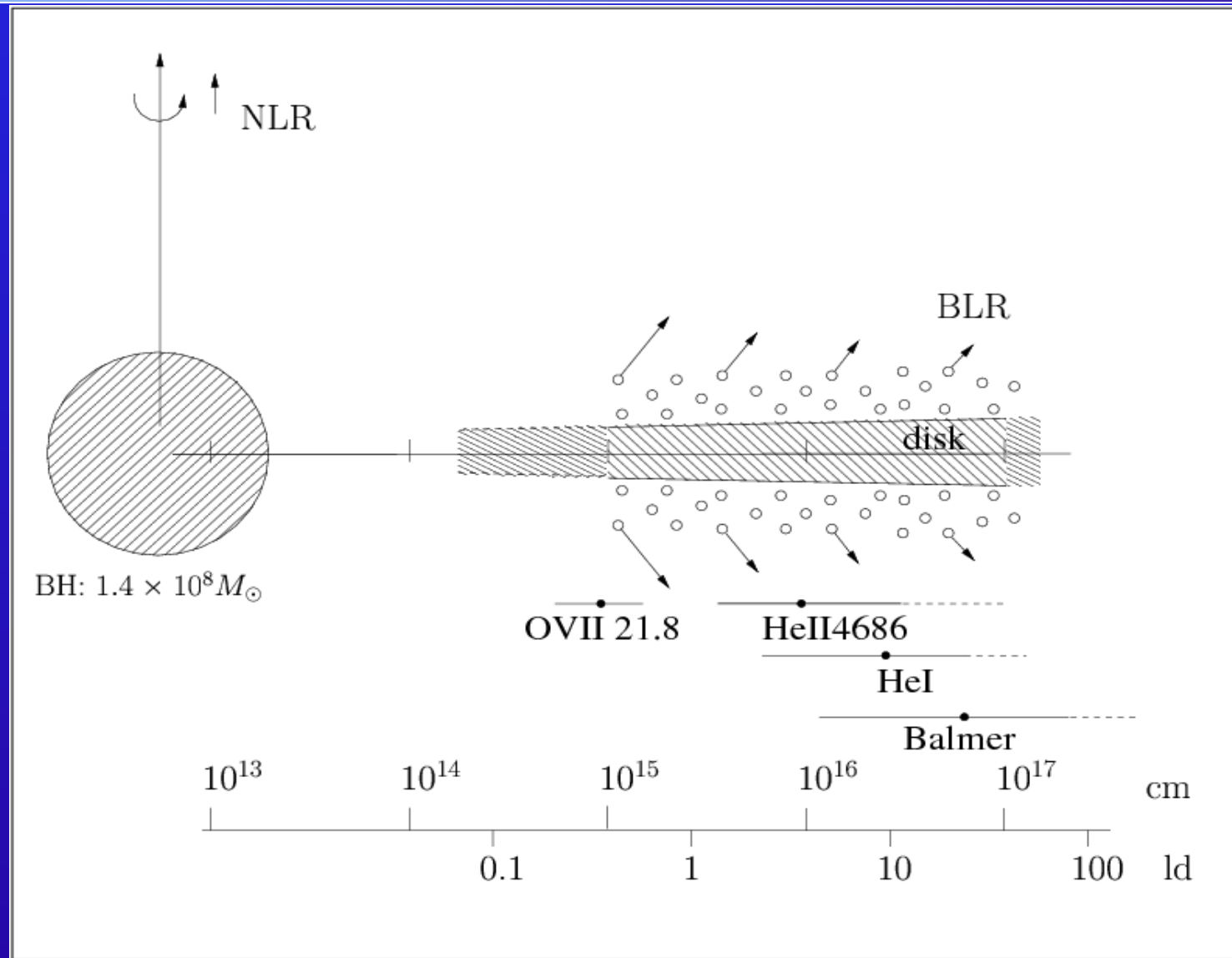
long-term continuum light curve <sup>Mrk110</sup> spectra taken between 1999 Nov. and



1987

<sup>2000</sup>  
9.2m Hobby-Eberly Telescope at McDonald Obs  
S/N >100

# The inner BLR structure in Mrk110



$$i = 21^{\circ} \pm 10$$

opt.:  $3.9 \text{ light-days } (\hat{=} 9.8 \cdot 10^{15} \text{ cm}) = 230 \text{ Schwarzschild radii } r_s$

X-ray:  $0.34 \text{ ld} = 21 r_s$

$$(r_s = 2GM_{grav}/c^2)$$

# Theory : BLR kinematics - line profile variations

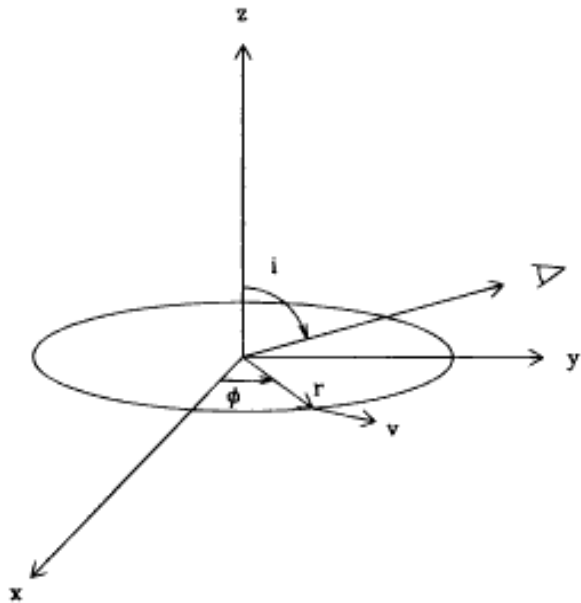


FIG. 1.—Geometry of the disk broad-line region. The angle,  $i$ , is the disk inclination relative to the observer. The quantities  $(r, \phi)$  label locations on the disk.

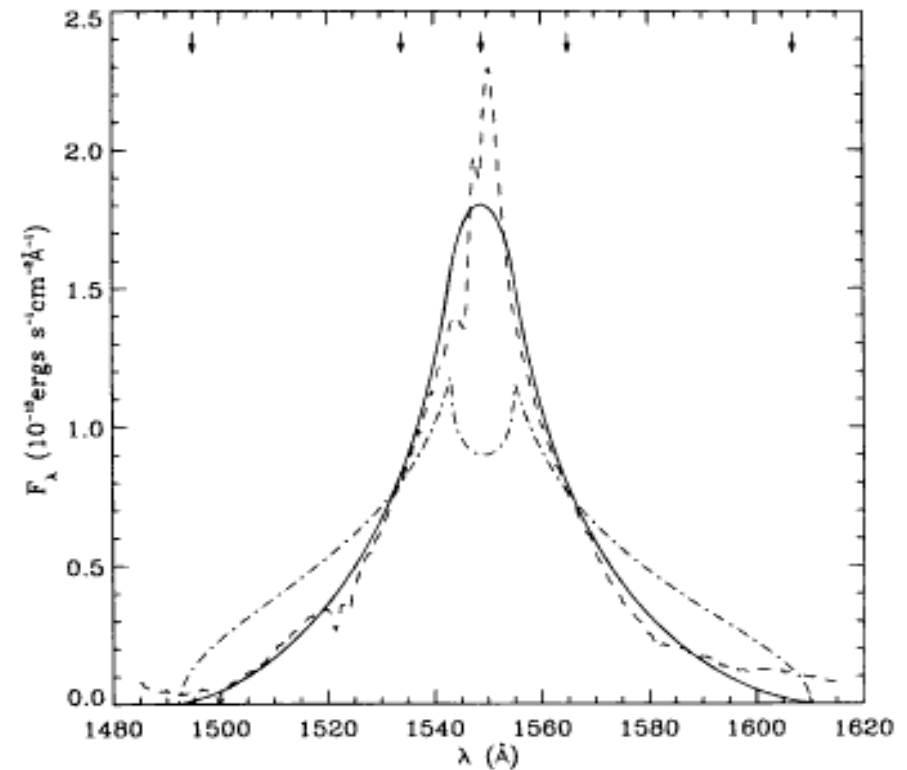


FIG. 2.—Data and model line profiles for the C IV line of NGC 5548. The solid line is the model calculation including the effects of the anisotropic emission. The dashed line is the data from the 1994 *HST* observations described by Korista et al. (1995). Also shown is the double-peaked profile (*dot-dashed line*) of a model line calculation that assumes isotropic emission. The arrows indicate the boundaries of the various wing and core components.

optically thick accretion disk models: single lined profiles

Chiang & Murray, 1996



# Scale Sizes of an AGN

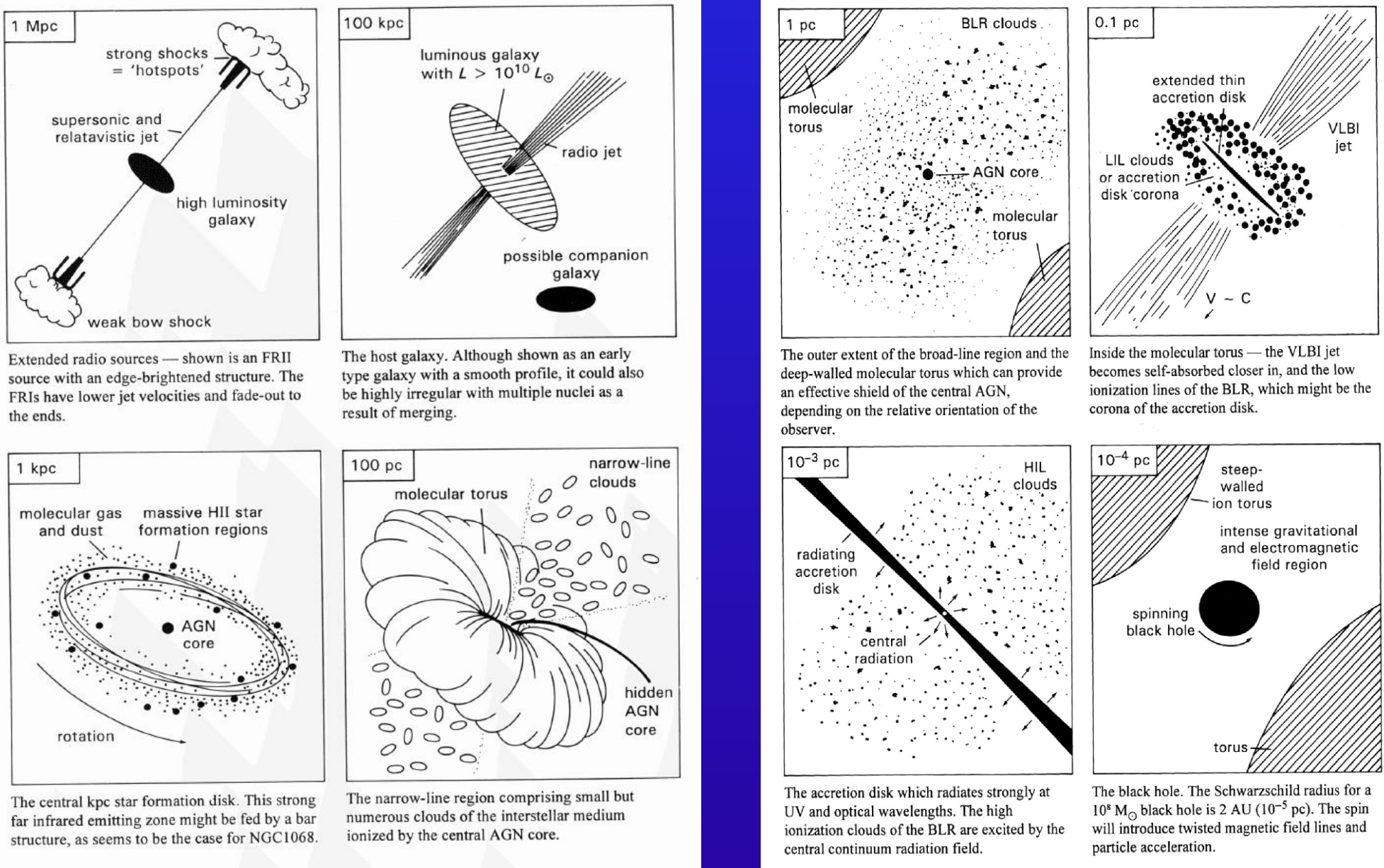


Fig. 9.9 Cartoon of the representative scale sizes of an AGN. How we eventually see the object depends on a number of parameters, the main one being the orientation of the obscuring torus with respect to the observer. (Adapted from Blandford, *Active Galactic Nuclei*, Saas-Fee Advanced Course 20, Springer-Verlag, 1990.)

HST :  $0.1'' \cong 2\text{pc}$

R. Blandford

$1\text{pc} = 3.3 \text{ ly} = 1190. \text{ Id} = 3 \cdot 10^{18} \text{ cm}$

# Central Black Hole Mass $M(\text{grav})$ in Mrk110

Central black hole mass in Mrk110 derived from gravitational redshift.

Observed shifts of rms profiles identified as gravitational redshift:

$$M_{grav} = c^2 G^{-1} R \Delta z$$

$R = c\tau$   $\tau$  = mean dist. of line em. clouds

Line	FWHM(rms) [km s <sup>-1</sup> ]	$\Delta v_{cent}$ (rms) [km s <sup>-1</sup> ]	$\tau$ [days]	$M_{grav}$ [10 <sup>7</sup> $M_{\odot}$ ]
(1)	(2)	(3)	(4)	(5)
HeII	4444. $\pm$ 200	541. $\pm$ 60	3.9 $\pm$ 2.	13. $\pm$ 3.
HeI	2404. $\pm$ 100	186. $\pm$ 60	10.7 $\pm$ 6.	12. $\pm$ 4.
H $\beta$	1515. $\pm$ 100	118. $\pm$ 50	24.2 $\pm$ 4.	17. $\pm$ 4.
H $\alpha$	1315. $\pm$ 100	74. $\pm$ 50	32.3 $\pm$ 5.	14. $\pm$ 5.

$$M_{grav} = 14. \pm 3 \cdot 10^7 M_{\odot}$$

# Theory : BLR kinematics - line profile variations

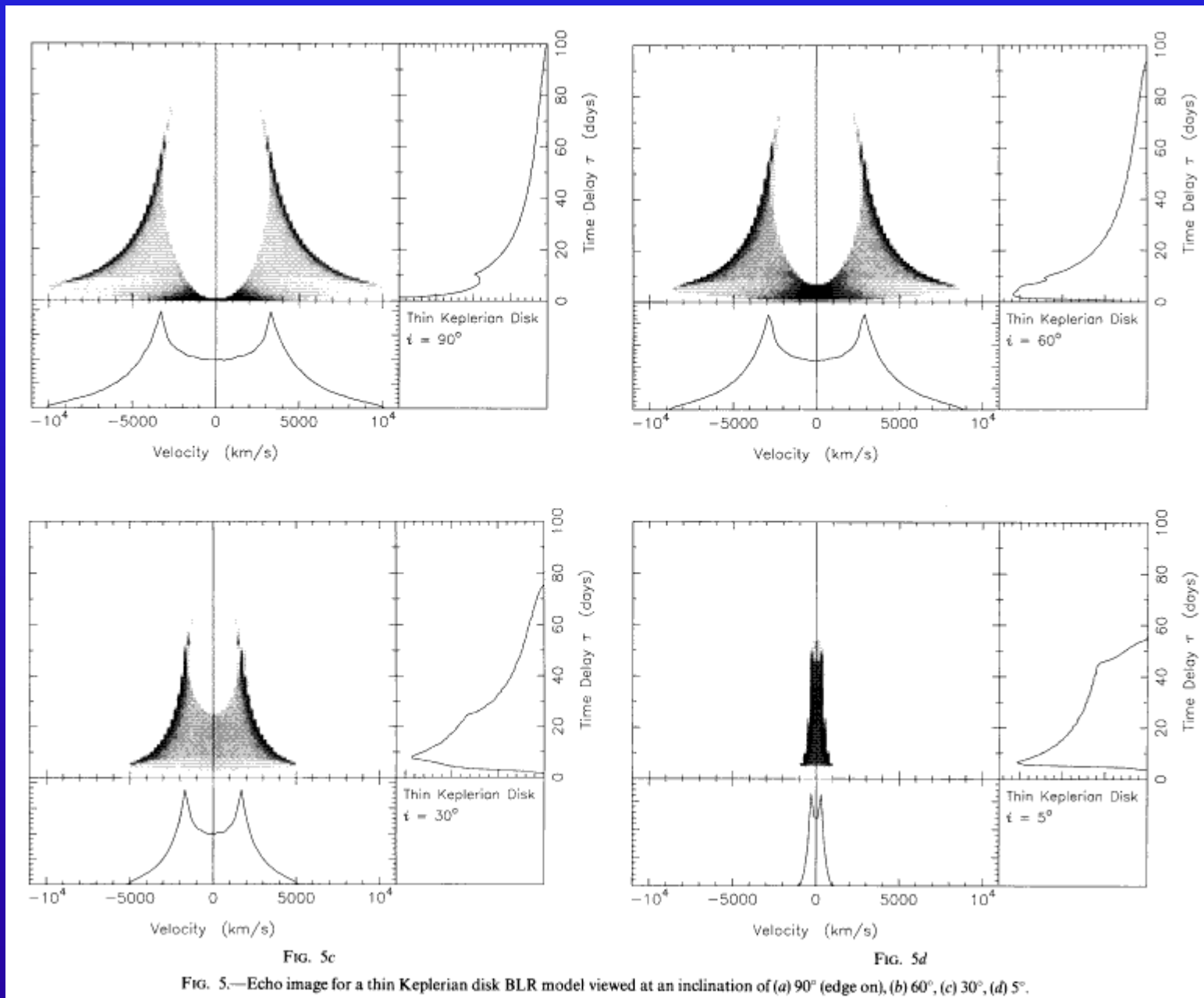
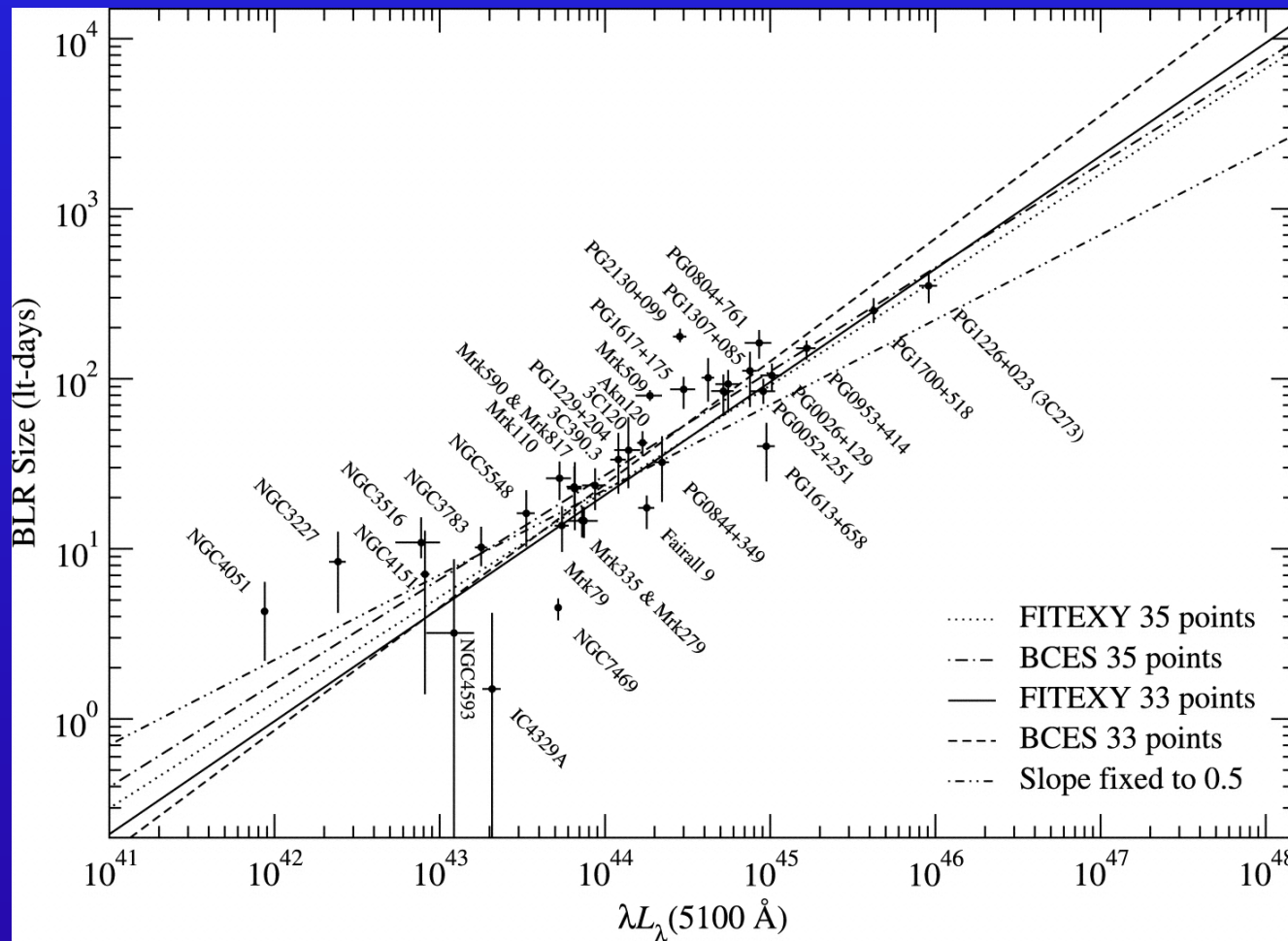


FIG. 5.—Echo image for a thin Keplerian disk BLR model viewed at an inclination of (a)  $90^\circ$  (edge on), (b)  $60^\circ$ , (c)  $30^\circ$ , (d)  $5^\circ$ .

Velsh & Horne, 1991

velocity-delay maps (echo images) for thin Keplerian disk BLR mod. viewed at inclination angles of 90 deg (edge on), 60, 30, 5 deg.

# Balmer line averaged BLR size in AGN



photoion. theory:

$$r = \left( \frac{Q(\text{H})}{4\pi c n_e} \right)^{1/2} \propto L^{1/2}$$

hydrogen-ionizing photons emitted

relationship between luminosity and broad-line region size

scatter due to: BLR density, column density, ionizing spectral energy distribution

Kaspi et al. 2004